Article

Adsorptive Effect of Corn Silk-Loaded Nickel Oxide and Copper Oxide Nanoparticles for Elimination of Ciprofloxacin from Wastewater

Chisom Theresa Umeh,* John Kanayochukwu Nduka, Kovo Godfrey Akpomie, Joshua O. Ighalo, and Refilwe Mogale

Read Online

ACCESS | Metrics & More | Article Recommendations

ABSTRACT: Ciprofloxacin (CIP) is one of the most reported antibiotic pollutants in hospital and industrial wastewater systems. The inclusion of nanosized transition metal oxides in adsorbent materials is able to improve the affinity and aqueous phase uptake of CIP from water. In this study, we report for the first time composites of corn silk with impregnated nanoparticles of NiO (NiONPs-CS) and CuO (CuONPs-CS) for the removal of CIP from water. The adsorbent was characterized using scanning electron microscopy (SEM), Fourier transform infrared (FTIR), energy-dispersive X-ray spectroscopy (EDX), an adsorption/desorption analyzer, and X-ray diffractometer (XRD) to study the morphology, surface functionality, elemental composition, textural properties, and crystal phases. The monolayer adsorption capacities of NiONPs-CS and CuONPs-CS were 108.3 and 120.2 mg/g, which were over 2 times higher than the capacity for unloaded corn silk. The kinetics of the adsorptive uptake followed the pseudo-second-order kinetics, revealing that both adsorption site density and CIP aqueous concentration control the removal rate. NiONPs-CS and CuONPs-CS were reusable for five cycles, with the uptake efficiency being 63.1 and 66.9%, respectively. This dropped to 47.8% for the unloaded corn silk. The mechanism of uptake was mainly by electrostatic attraction, pi−pi interaction, hydrogen bonding, and hydrophobic interaction. Based on our findings, the adsorbents have proven to be an efficient, cheap, and reusable material for CIP uptake.
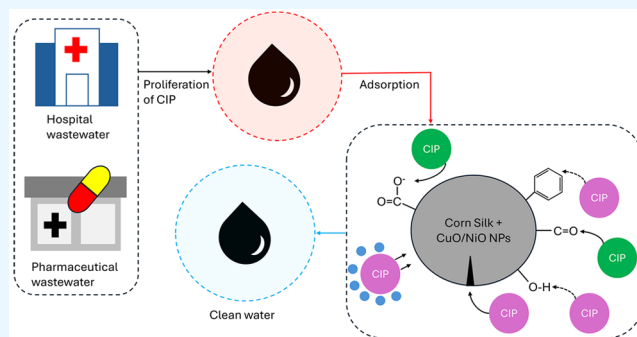
INTRODUCTION

Water is important for our daily activities; thus, the quality of water resources we depend on is affected by population growth and the incessant increase in production with accumulation of emerging pollutants, drastically decreasing the water quality.[1] These toxic pollutants keep accumulating alongside related problems in water bodies.[2] Hospitals are the most water consuming establishment among the water consumption sectors after industrial and manufacturing sectors of the economy, and the used water is being converted into sewage. Effluents from hospitals contain suspended particulates, biodegradable organic compounds, some toxic heavy metals, pathogens, antibiotic drug residues/remnants, disinfectants, radioactive isotopes, and detergents.[3,4] Among the emerging pollutants are antibiotics that can cause severe health effects when the residues from human urine and feces as well as pharmaceutical industries are released into water bodies via the wastewater system.[5] Some of these antibiotics are absorbed partially in the human body, and the rest about 30−90% of them are defecated without being digested into the sewage plant.[6] Due to the fact that some of these antibiotic drugs are

nonbiodegradable and stay in the environment for long time, the aquatic ecosystem becomes contaminated with reduced reproductive functions of aquatic lives.[7,8] Most health impairment, such as reduced sperm count, increased prostrate and breast cancer, and damaged DNA and lymphocytes, can emanate from low concentrations of antibiotics.[9] Among the fluoroquinolone antibiotics, ciprofloxacin (CIP) is one of the most commonly used for the treatment of bacterial infections that are found in household, hospital, and pharmaceutical wastewater systems. Incomplete decomposition of CIP by the body can lead to an increased pollution of clean surfaces and groundwater when in contact with the sludge, which can be toxic to the ecosystem and cause negative public health
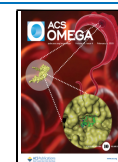
outcomes.[10] Again, the existence of ciprofloxacin in water bodies can result in formation of antibiotic-resistant bacteria, which might reduce the level of oxygen in water when heavily accumulated, thus leading to increased health issues via food chain.[11] Also, the sludge containing the ciprofloxacin antibiotic when used as a fertilizer can be absorbed and accumulated in the soil and enter plants, thus reducing some physicochemical functions of affected plants.[12] The treatment of drug-resistant bacteria is capital-intensive and time-consuming; hence, there is a need for the efficient removal of the ciprofloxacin antibiotic from aqueous media. There are different promising wastewater treatment technologies, such as adsorption, anaerobic reactors, membrane bioreactors, sonochemical, photocatalytic, sonocatalytic, and reverse osmosis processes for the treatment of effluents containing antibiotics.[13,14] Apart from the adsorption process, these methods have been found to have drawbacks in terms of removal efficiency, high treatment costs, complexity, and other needs for further monitoring.[15] The adsorption method tends to be the most preferred treatment process owing to its capacity and effectiveness in sequestration of toxic substances, economic benefits, delivery of high-quality treated water when applied using a well-designed plant system, and control of sludge disposal to the environment.[16]

Nanotechnology appears to be a convenient and promising alternative for pollutant uptake by the adsorption mechanism.[17] The eco-friendly green synthesis of nanoparticles (NPs) via biological sources proves their efficiency in the effluent treatment field due to their cost-effectiveness, accessibility, and less toxicity to health, environment, and other organisms.[18] Availability, biodegradability, antibacterial potential, biocompatibility, and hydrophilicity are some vital properties that give plant-based nanomaterials a discrete advantage over other supported materials.[19] Nanoparticles (NPs) are categorized by small sizes of about 1−100 nm that enable their high surface area-to-volume ratio to improve reactivity together with their solubility, mobility, interface effects, and quantum features.[20] Nanomaterials find useful applications in environmental, biological, engineering, climate change, and medical sectors due to their innovative physical and chemical properties.[21] The next-generation adsorbents (nanoadsorbents) for water treatment systems overcome the limitations of conventional adsorbents such as challenges in separation of adsorbents from treated water, inconvenience in removing pollutants at the part per billion (ppb) level, and surface functionalization that require complex synthesis processes and are costly for large-scale processing.[22] Nanoadsorbents possess high capacity being practical units to eliminate organic and inorganic contaminants from air and wastewater by adsorption.[23] The use of synthesized nanoparticles (NPs) for the efficient adsorption of antibiotics and other pollutants has been demonstrated by recent research trends.[24−31] Several techniques such as coprecipitation, sol−gel, green synthesis, hydrothermal, vapor deposition and chemical reduction can be utilized to generate NPs.[32−34] Due to toxicity and low reusability, the application of noble metal NPs based on central atoms is limited.[35] The aforementioned drawbacks can be overcome by formation of a nanocomposite via impregnation or loading of these metallic NPs on a substrate to form a composite adsorbent, which improves the adsorption drugs and other toxic pollutants.[36,37] Nickel oxide and copper oxide NPs are among the important transition metal oxide materials with cubic lattice (NiO) and monoclinic (CuO) structures used in all sort of applications.[38,39] This nickel oxide NPs possess unique features such as physical, chemical, optical, electrical and thermal and cyclic reversibility.[40] Copper oxide NPs has received remarkable consideration owing to their narrow band gap, low cost, desirable textural properties, high surface area, cytotoxicity, antimicrobial activities, catalytic activity, abundant active sites, and efficient adsorption capacity.[41] Recent efforts are being made to explore the probable utilization of these metal oxide nanoparticles for socio-economic growth.

A thorough literature search showed that corn silk adsorbent surface impregnated with Ni and Cu oxide NPs to form a nanocomposite has not yet been reported for the adsorption of ciprofloxacin. As a renewable biowaste, corn silk is a fibrous material rich in steroids, polyphenols, proteins, and volatile oils with some functional groups such as carbonyl, carboxyl, and hydroxyl that make it ideal for organic contaminant removal from wastewater via adsorption. Hence, this study aimed to investigate the impregnation of NiO and CuONPs on corn silk (CS) to form novel metal composites (NiONPs-CS and CuONPs-CS) applied for the sequestration of the CIP antibiotic from aqueous solution. The detailed characterization using scanning electron microscopy (SEM), Fourier transform infrared (FTIR), energy-dispersive X-ray spectroscopy (EDX), Brunauer−Emmett−Teller (BET), and X-ray diffractometer (XRD) analysis was studied to understand the morphology, surface functionality, elemental composition, pore size, and crystallinity properties of dual nanocomposites. The effect of operational parameters on CIP removal was studied together with the point of zero charge, isotherms, kinetics, and thermodynamics of biosorption. The efficiency of the novel adsorbents was further examined through a regeneration study.

■ MATERIALS AND METHODS

Preparation of Biomass. Corn silk samples were collected from local farmland and washed twice with double-distilled water. 100 g of the plant was cut into equal size and then sundried for 48 h, followed by oven-drying at 80 °C for 2 h in a laboratory oven. The dried samples were crushed to powder using a mortar and pestle, followed by the addition of 200 mL of 0.1 M HNO_3 to 40 g of the powder. The mixture was stirred for 1 h and then washed with distilled water until pH 7.0, followed by oven-drying at 70 °C for 24 h. The pulverized samples were passed through a 100 μm mesh screen to obtain the desirable particle sizes.

Preparation of Nickel Oxide and Copper Oxide Nanoparticle-Loaded Corn Silk. The synthesis of NiONPs-CS and CuONPs-CS adsorbent composites was done following some part procedures of magnetite nanoparticles on *Musa acuminata* peels[24] and ZnONPs impregnated pea peels.[42] The nanocomposites were prepared by a thermochemical precipitation reaction in solution by first dissolving 5.26 g of $NiSO_4·6H_2O$ and 5 g of $CuSO_4·5H_2O$ separately in 100 mL of distilled water on a hot plate and stirred for 30 min at 30 °C to ensure complete dissolution of the salts. Then, 10 g of the prepared CS was added to separate salt solutions with constant stirring for 2 h. A color change from bright green to dark green and light blue to dark blue was observed for NiO and CuO nanoparticles. This was followed by the addition of a few drops of 0.5 M NaOH until the solution pH was 11 with further stirring for 8 h. Thereafter, the mixtures were then centrifuged at 4000 rpm for 2 h. This was followed by washing with excess water until pH 7.0, centrifuging, and then oven-drying at 70 °C for 24 h. The
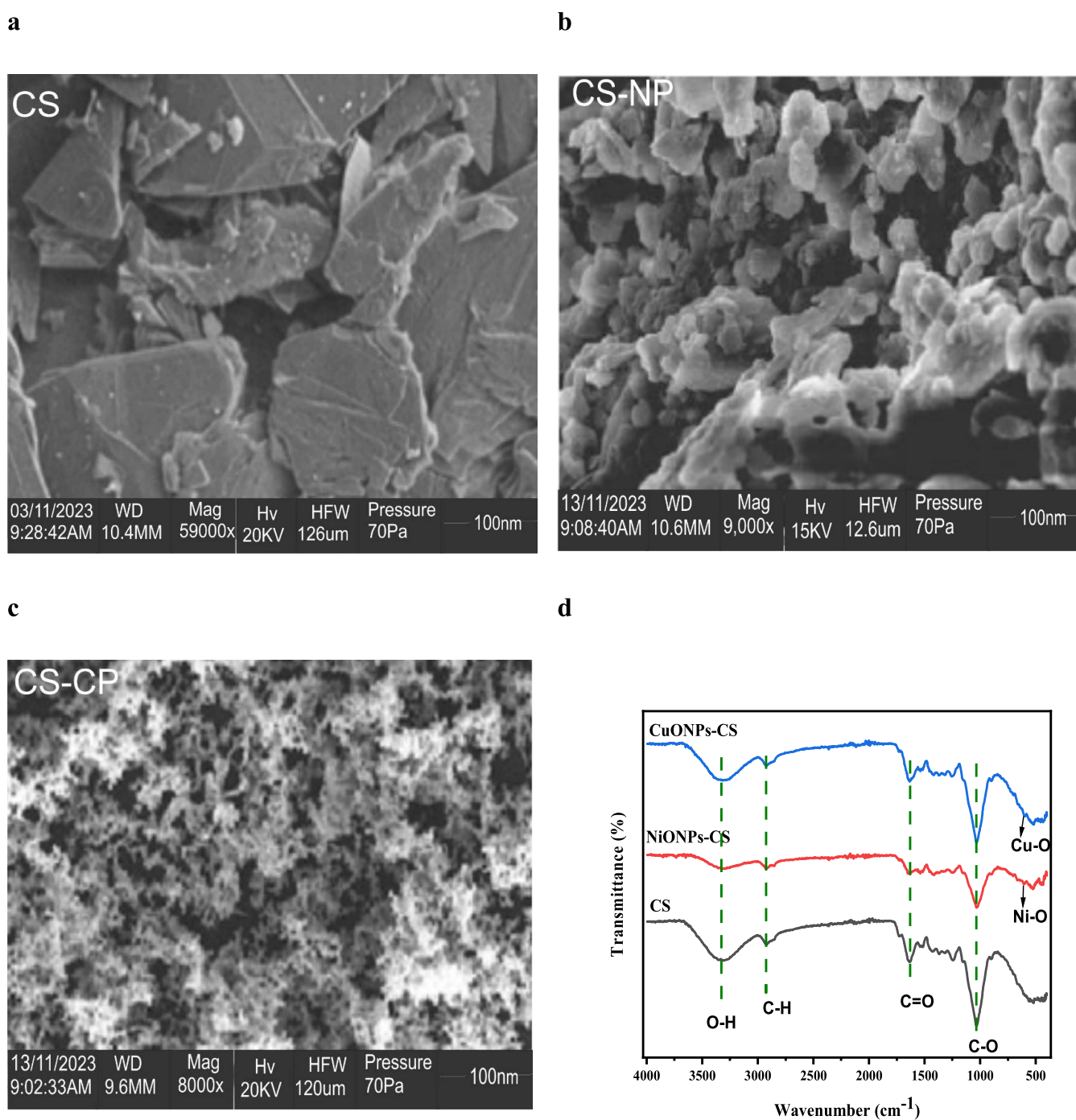
a

b

c

d

Figure 1. Scanning electron microscopy of (a) CS, (b) NiONPs-CS, and (c) CuONPs-CS at 100 nm, and (d) Fourier transform infrared spectra of CS, NiONPs-CS, and CuONPs-CS.

residues were pulverized and passed through a 100 μm mesh screen to obtain the as-prepared NiONPs-CS and CuONPs-CS composites.

The following devices were used for the analysis of the nanocomposites: Fourier transform infrared (FTIR) spectroscopy (Bruker Tensor 27 IR), thermogravimetric analyses (TGA), a Mettler Toledo TGA/SDTA 851, a scanning electron microscope (SEM/EDS-JEOL-JSM-7600F), an X-ray diffractometer (XRD Rigaku D/MaxlllC, PW 1800), and a surface area and porosity analyzer (ASAP 2020). Surface area and porosity measurements were obtained with a micrometric analyzer, and their relevant indicators were calculated using the

Brunauer−Emmett−Teller (BET) equation and the Barrett−Joyner−Halenda (BJH) method.

Adsorption Study. Batch adsorption experiments were performed in a 100 mL conical flask containing a specified amount of prepared nanocomposites. The CIP drug used was obtained from Neros Pharmaceutical Company, Nigeria. First, 0.5 g of CIP powder was mixed with distilled water to prepare 500 mg/L stock solution, and then, the aqueous solution was further diluted serially with different concentrations for conducting experiments. This study was performed by including five factors, e.g., contact time (from 20 to 60 min), the amount of nanocomposites (from 0.1 to 0.5 g) at pH

between 3 and 9, reaction temperature of 30−70 °C, and concentrations of 20−100 mg/L. In this study, the optimal value of each parameter was obtained. A UV−vis spectrometer (725N, Japan) was used to measure the CIP concentrations in the filtrate according to the usual technique at a wavelength of 280 nm. The amount of equilibrium adsorption, q_e, and percentage removal, % R were calculated with eqs 1 and 2[43]

$$q_e = \frac{(C_o - C_e)V}{M} \tag{1}$$

$$\% R = \frac{C_o - C_e}{C_o} \times 100 \tag{2}$$

Desorption Experiment. Considering the recovery of the pharmaceutical drug and regeneration of nanoadsorbents, the CIP drug was desorbed from NiONPs-CS and CuONPs-CS using 0.1 M HNO$_3$ as the eluting solvent. Then, desorption suspensions were stirred for 1 h at room temperature and centrifuged at 4000 rpm for 30 min. The supernatants were subjected to UV and AAS for the quantification of the desorbed pollutants. The separated NiONPs-CS and CuONPs-CS were washed with distilled water four times and used for resorption after oven-drying at 105 °C for 3 h. The adsorption−desorption experiment was conducted for five cycles to investigate the reuse potential of NiONPs-CS and CuONPs-CS based on the measured efficiency. Desorption efficiency was computed using eq 3[44]

$$d_E (\%) = \frac{q_{de}}{q_{ad}} \times 100 \tag{3}$$

where d_E is the desorption efficiency (%), q_{de} is the desorbed concentration, and q_{ad} signifies the adsorbed concentration of the heavy metal and dye onto ACS powder.

Statistical Error Analysis. To estimate a better fit or accuracy in determining which of the isotherm models is best to describe the adsorption process, three statistical error functions were utilized as shown in the following equations.[4,45]

$$\text{sum square error (SSE)} = \sum_{i=1}^{n} (q_{e,calcd} - q_{e,exp})_i^2 \tag{4}$$

$$\text{sum of absolute error (EABS)} = \sum_{i=1}^{n} |q_{e,exp} - q_{e,calcd}| \tag{5}$$

$$\text{Chi-square test } (\chi^2) = \sum_{i=1}^{n} \frac{(q_{e,exp} - q_{e,calcd})^2}{q_{e,exp}} \tag{6}$$

Here, $q_{e,exp}$ is the experimental value, while $q_{e,calcd}$ is the calculated value from the isotherm models, and n is the number of observations in the experiment.

■ RESULTS AND DISCUSSION

Characterization of CS, NiONPs-CS, and CuONPs-CS. The surface morphology of CS, NiONPs-CS, and CuONPs-CS revealed in SEM images presented the transformation of the irregular surface structure to more numerous porous surface sites, as shown in Figure 1a−c. The unmodified adsorbents showed flaky microparticles of different shapes having rough surface structures. The impregnation of NiO and CuO nanoparticles on the surfaces of NiONPs-CS and CuONPs-CS after modification, which is absent in untreated CS,

depicted a clear transformation of the microstructure of the adsorbent. Most of the active sites were observed to have been occupied by the nanoparticles, hence the seemingly more homogeneous appearance. All cavities on the surface have been occupied by the NPs or target pollutants.

The identification of functional groups present in the raw and modified biomass was achieved using FTIR spectroscopy to promote the adsorption of CIP from aqueous media; from this measurement, as observed in Figure 1d, peaks at 3317, 2920, 1635, and 1033 cm^{-1} attributed to O−H, C−H, C=O, and C−O stretching bands, respectively, which are characteristics of cellulose, lignin, and pectin, are present in corn silk biomass. After impregnation of NiO and CuO nanoparticles, there was a decrease in the peak values, size, and intensity of the absorption bands, which indicates the occupation of the surface functional sites by the loaded nanoparticles. The presence of vibrational bands at 668 and 627 cm^{-1} is characteristic of Cu−O and Ni−O functional groups, respectively. The successive formation of Cu−O was confirmed by the presence of absorption peaks at the range of 500−700 cm^{-1} as previously reported.[46,47] As observed again, the broad and intense peaks at 516 and 526 cm^{-1} were ascribed to the stretching vibrations of Cu−O and Ni−O vibrations due to copper and nickel oxide functional groups, respectively. A similar scenario was reported by Prajapati and Mondal[26] on adsorption of methylene blue using CuONPs showing a peak at 519 cm^{-1} that indicated Cu−O bonding. The existence of these observed functional groups on the CS, NiONPs-CS, and CuONPs-CS as identified by the FTIR simply depicts the efficiency of these biosorbents to interact with CIP molecules in solution.

The thermal behavior of CS, NiONPs-CS, and CuONPs-CS was estimated by thermogravimetric analysis, as shown in Figure 2. The studied adsorbents demonstrated significant weight loss from 250 to 420 °C, indicating the removal of moisture and decomposition of organic matter.[48] The impregnation of the nickel and copper oxide nanoparticles on the raw biomass increases the thermal stability of CS, as indicated by the lower weight loss of the prepared NiONPs-CS
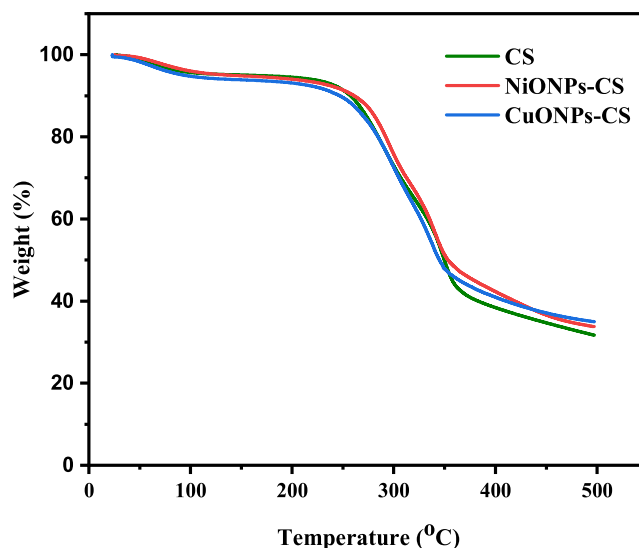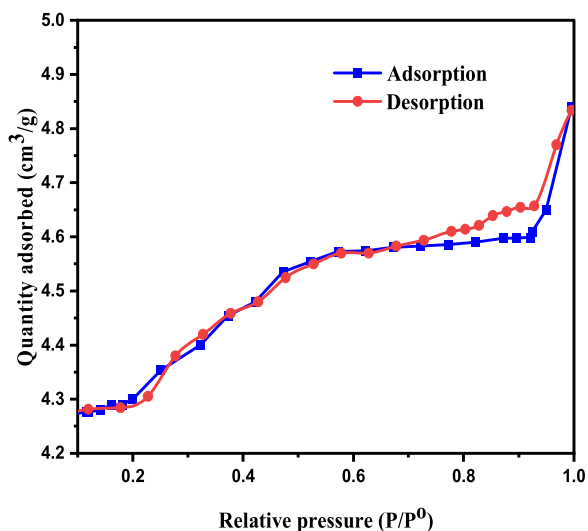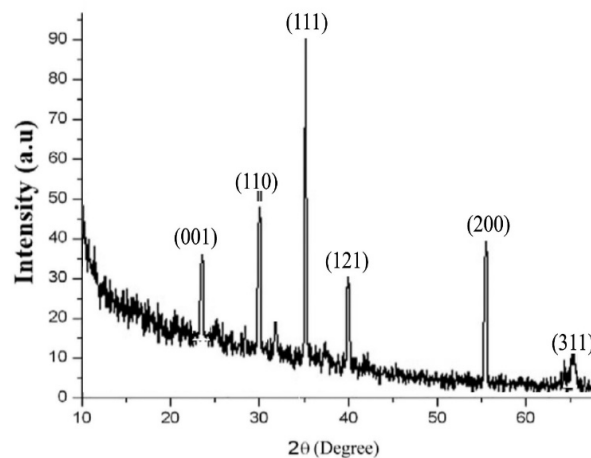

Figure 2. Thermogravimetric analysis of CS, NiONPs-CS, and CuONPs-CS.

(a) NiONPs-CS
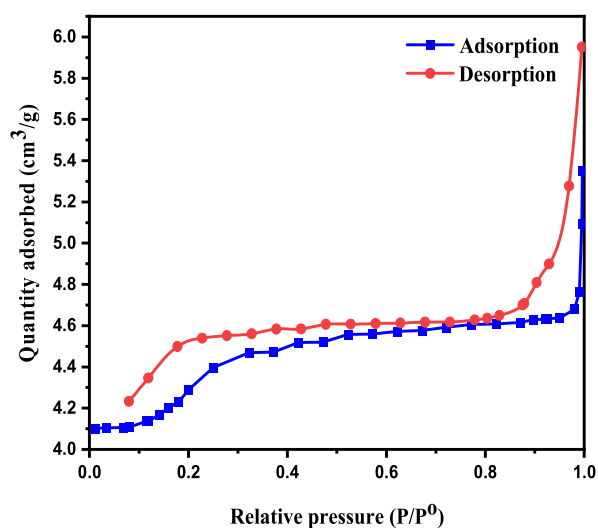

(b) NiONPs-CS

(c) CuONPs-CS
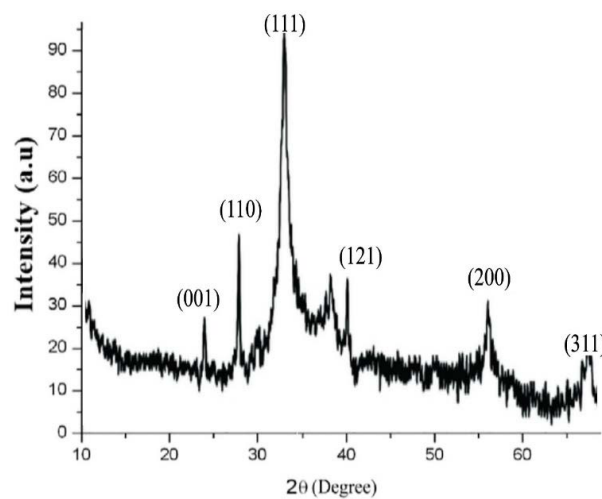

(d) CuONPs-CS

Figure 3. (a) Nitrogen adsorption−desorption isotherm and (b) X-ray diffraction of NiONPs-CS; (c) nitrogen adsorption−desorption isotherm and (d) X-ray diffraction and CuONPs-CS.

and CuONPs-CS with temperature, depicting reduced decomposition compared to that for CS.

The porosity of CS, NiONPs-CS, and CuONPs-CS could be analyzed by nitrogen adsorption−desorption isotherms and distribution of pore size.[49] As shown in Figure 3a,c, the isotherms of CuONPs-CS and NiONPs-CS nanosorbents partially displayed IV-type shapes, indicating that there was a hysteresis loop. This is due to capillary condensation and verifies mesoporosity. The BET specific surface areas for adsorbents were 0.42, 0.47, and 1.10 m^2/g for corn silk, NiO, and CuO corn silk composites, respectively. The specific surface of the raw biomass increased when the samples were treated with NiO and CuO nanoparticles to obtain the composites with higher surface areas. Moreover, a total pore volume of 0.003 cm^{-1} and a pore size of 6.10 nm were

obtained for copper oxide-loaded composites, according to the Barrett−Joyner−Halender method (BJH), which are higher than those for nickel oxide-impregnated composite (0.001 cm^{-1} and 1.77 nm, respectively). Nevertheless, the pore volume and pore size of the nanocomposites were more than those of the raw plant biomass, which makes them beneficial for the uptake of pharmaceutical CIP antibiotics.

The XRD spectra of the impregnated biosorbents were used to identify the phases and crystalline nature of the adsorbents, as shown in Figure 3b,d. The diffraction peaks at 2θ values of 24.26, 30.65, 36.24, 40.22, 52.16, and 66.25°, respectively, correspond to the (001), (110), (111), (121), (200), and (300) monoclinic phases of the NiO-loaded adsorbent and 2θ values at 23.22, 28.47, 33.22, 40.22, 52.21, and 68.02°, respectively, correspond to the (001), (110), (111), (121),
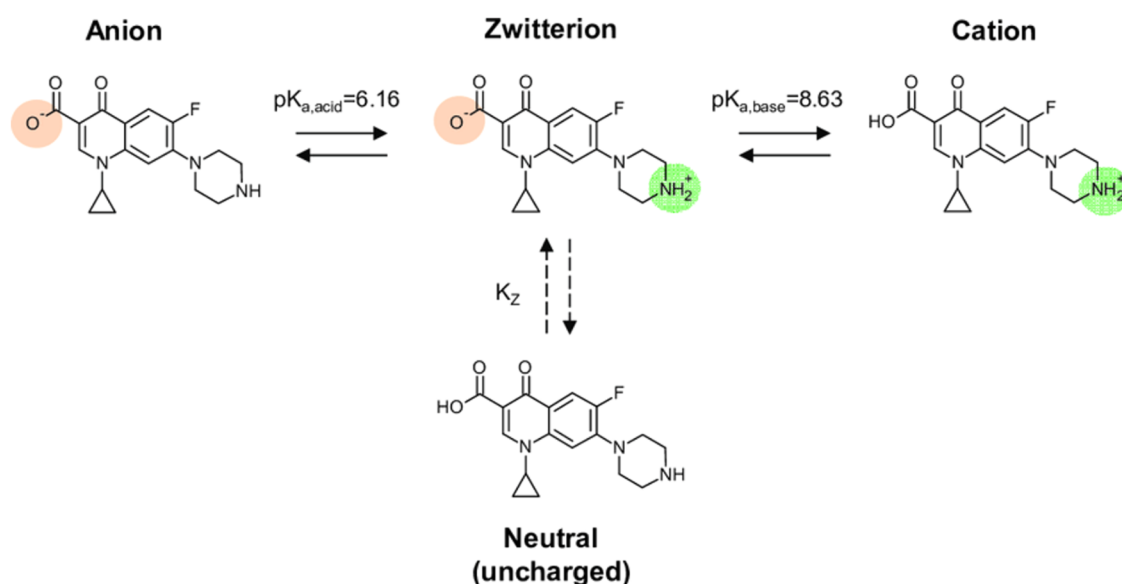
Figure 4. Ionized species of ciprofloxacin.

(200), and (300) monoclinic crystalline planes of CuO nanoparticles, as indexed in JCPDS-No 48-1548.[50] An intense peak at 43.30° corresponding to the (111) crystalline plane for NiO and CuO nanoparticle-mediated Curcuma longa was reported in a study of antimicrobial activities.[51] The average crystalline sizes were calculated as 9.3 nm for NiONPs-CS and 18.1 nm for CuONPs-CS from the Debye−Scherrer formula ($D = k\lambda/\beta\cos\theta$), which are higher than that for the raw CS (1.12 nm) reported in a previous study,[45] depicting the successive formation of target metallic oxide nanoparticles for adsorption efficiency.

Effect of Solution pH. The initial pH of the effluent has a significant impact on the adsorption of pharmaceutical drugs because it affects ionization, drug solubility in binding with hazardous compounds, and the surface chemistry of the adsorbent.[52] Ciprofloxacin is an amphoteric organic molecule having weak alkaline dimethylamine and weak acidic phenolic hydroxyl. The pK_a values of CIP are pK_{a1} 6.16 and pK_{a2} 8.63, as shown in Figure 4.[53] When the pH value is less than 6.16, the CIP molecule is mainly present in the form of a cation (CIP^+) due to protonation of the amine group, whereas when the pH is higher than 8.63, the anionic CIP (CIP^-) is predominant as a result of deprotonation of the carboxylic group.[54] The attraction between the adsorbent particles and adsorbent molecules is expected to be higher at a pH range of 6.16−8.63 as their surfaces are of opposite charges, hence a necessity in evaluating the effect of initial pH on CIP uptake.

The current study shows the varying effect of pH for the uptake of CIP onto CS, NiONPs-CS, and CuONPs-CS nanocomposites depicted in Figure 5a, the change in solution pH from 3.0 to 9.0 significantly influence the adsorption of CIP. The removal efficiency of the target pollutant was low when the pH of aqueous solution was at the acidic level but increased when the pH values of the solution increased toward the basicity range. Higher adsorption capacity was attained at pH of 6, 7, and 9, which are within the pK_{a1} and pK_{a2} constants. This depicts that the higher pH of the solution was favorable for CIP adsorption owing to more reacting ammonium substrates of the drug. High drug removal at higher pH (alkalinity) is attributed to the electrostatic attraction between the negatively charged adsorbent surface and positive

CIP molecules in solution. It is clearly observed that NiO and CuO impregnation increases the CIP uptake at different pH values compared to raw CS.

The points of zero charge (pH_{pzc}) of NiONPs-CS and CuONPs-CS were assessed to be 6.2 and 7.4 (Figure 5b). When the pH values are lower than pH_{pzc}, the adsorbent materials possess positively charged surfaces, and when the pH values > pH_{pzc}, they have a negatively adsorbent surface. The nanocomposites covered by negative charges of OH^- attract CIP^+ molecules, while positive charges of H^+ attract CIP^- molecules. Therefore, the lower adsorption efficiency obtained at acidic pH values is due to the fact that pH < pH_{pzc}. CIP^+ is predominant in the aquatic environment,[6] meaning that electrostatic attraction can occur between the negatively charged adsorbent and pollutant ions at pH values > pH_{pzc}. The interaction mechanisms of $\pi-\pi$ and n−π electron donor−acceptor with benzene rings actually participated in the adsorption of the studied organic compound adsorbate. The benzene ring in the CIP structure acts as an electron acceptor due to the existence of a highly electronegative fluorine group.[55,56]

Effect of Adsorbent Dose. Another important adsorption process is the adsorbent dose, which is associated with the availability of vacant active sites. The increase in the mass of the adsorbent in aqueous media will result in the higher uptake of the adsorbate as a result of the high surface area of the adsorbents, leading to more binding sites of the adsorbing materials.[25] The effects of raw plant biomass and nano-synthesized dosage on the removal of ciprofloxacin are illustrated in Figure 5c. When adsorbent dosage increased from 0.1 to 0.5 g, the percentage of CIP removal increased from 63.5 to 73.8%, 70.5 to 75.8%, and 70.1 to 72.9% for raw CS, NiONPs-CS, and CuONPs-CS, respectively. The prepared nanocomposites presented higher CIP uptake than CS in the studied dosage range, which reflects the suitability of NiONPs and CuONPs impregnation in improving the adsorption of antibiotic drug molecules onto CS. Nevertheless, the effective removal of CIP decreases significantly from 34.9 to 8.1, 38.8 to 8.3, and 38.6 to 8.0 mg/g for CS, NiONPs-CS, and CuONPs-CS, respectively. The decreasing effect is a result of more available binding sites and collision between biosorbent
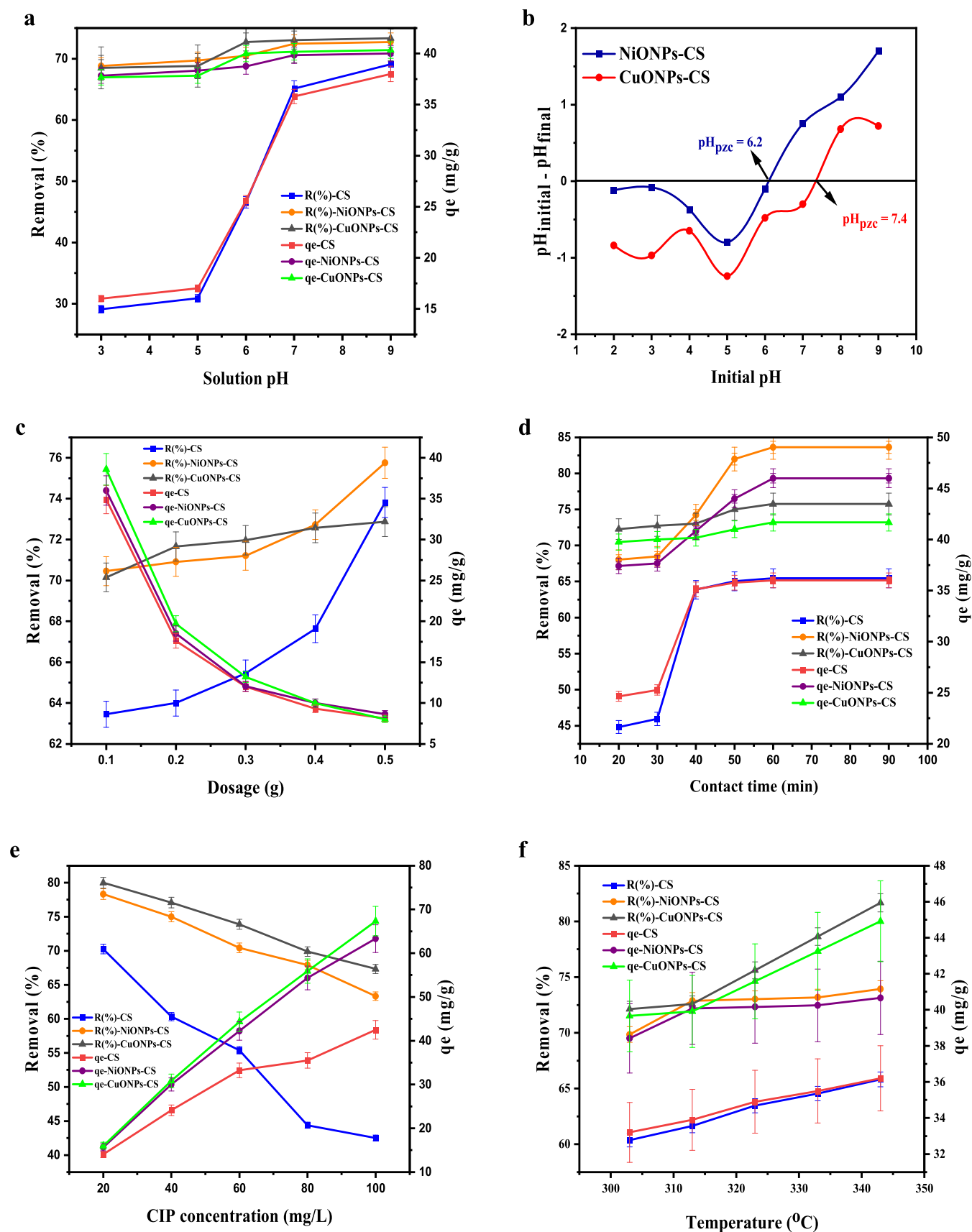
Figure 5. (a) Effect of pH, (b) point of zero charge, (c) effect of adsorbent dosage, (d) effect of contact time, (e) effect of CIP concentration, and (f) temperature on adsorption of CIP onto CS, NiONPs-CS, and CuONPs-CS.

Table 1. Isotherm Parameters for the Adsorption of CIP on CS, NiONPs-CS, and CuONPs-CS

models	parameters	CS	NiONPs-CS	CuONPs-CS
Langmuir	K_L (L/mg)	0.056	0.038	0.038
$\frac{C_e}{q_e} = \frac{1}{q_m K_L} + \frac{C_e}{q_m}$	q_m (mg/g)	53.53	108.34	120.19
K_L = Langmuir isotherm constant (L/mg)	R^2	0.9795	0.9950	0.9954
Q_m = maximum monolayer coverage capacity (mg/g)	SSE	12.796	2.884	2.767
	EABS	7.265	2.767	2.824
	χ^2	0.385	0.069	0.050
Freundlich	K_F (L/g)	6.284	6.222	6.498
$\log q_e = \log K_F + \frac{1}{n} \log C_e$	N	2.102	1.516	1.468
q_e, capacity adsorption (mg/g); K_F, Freundlich indicator of adsorption capacity (L/g); $1/n$, intensity of the adsorption indicating the surface heterogeneity and favorability of the adsorption process.	R^2	0.9750	0.9927	0.9939
	SSE	19.155	18.657	13.516
	EABS	7.970	8.087	0.294
	χ^2	0.581	0.372	7.474
Temkin	K_T (L/g)	0.52	0.42	0.44
$q_e = B \ln K_T + B \ln C_e$	B (J/mol)	12.05	22.42	24.11
B is the Temkin constant related to the heat of adsorption (J/mol), and K_T (L/g) is the equilibrium binding constant related to the maximum binding energy.	R^2	0.9751	0.9843	0.9825
	SSE	12.097	22.675	28.660
	EABS	7.178	10.193	11.330
	χ^2	0.364	0.740	0.882
Sips	$1/n$	2.15	2.71	2.73
$\ln\left(\frac{q_e}{q_{max} - q_e}\right) = \frac{1}{n} \ln C_e + \ln K_S$	q_m (mg/g)	42.70	63.55	67.55
K_s is the Sips equilibrium constant (L/mg), and $1/n$ is the Sips model exponent. If the value for $1/n$ is <1, it shows that it is a heterogeneous adsorbent, while values closer to or even 1 indicate that the adsorbent has relatively more homogeneous binding sites.	K_S (L/mg)	0.006	0.003	0.003
	R^2	0.7049	0.7507	0.7246
	SSE	93.506	302.574	353.643
	EABS	20.117	34.123	37.761
	χ^2	4.179	9.840	10.724
Dubinin and Radushkevich (D−R)	K_{DR} (mol²/kJ²)	7.72×10^{-6}	5.61×10^{-6}	4.98×10^{-6}
$\ln q_e = \ln q_m - K_{DR}\varepsilon^2$	q_m (mg/g)	35.47	51.42	53.99
$\varepsilon = RT \ln\left[1 + \frac{1}{C_e}\right]$	E (kJ/mol)	0.254	0.299	0.317
$E = \frac{1}{\sqrt{2K_{DR}}}$	R^2	0.8749	0.8757	0.8758
K_{DR} (mol²/kJ²) is a constant related to the mean adsorption energy, and ε is the Polanyi potential, R (8.314 J/mol·K) is the universal gas constant, T (Kelvin) is the absolute temperature, E (kJ/mol) is the mean free energy of adsorption.	SSE	97.834	309.738	355.873
	EABS	15.464	33.337	34.491
	χ^2	3.058	6.781	7.364

particles with dosage increase that leads to a less amount of the drug pollutant being adsorbed onto specific active sites.[57]

Effect of Contact Time. The reaction time of the adsorbent with the affecting target pollutant is another parameter in the area of adsorption technology. In this study, the desired contact time was recorded from 20 to 90 min, as can be seen in Figure 5d, and the adsorption capacity and percentage removal increased with reaction time. The uptake capacity and removal efficiency of CIP on raw CS were significantly lower than those on the NiO and CuO nanocomposites. In the first 20 min, the adsorbing materials have a large number of active sites and are ready to remove CIP very quickly. As shown in the second part of the curve (20−50 min), the adsorption rate increased because there were more available vacant sites than before with the increase in time. When the contact times were 60 and 90 min, the removal efficiencies of NiONPs-CS and CuONPs-CS composites were almost 83.64 and 75.76% higher than that of raw CS, respectively. Similar behavior was observed for adsorption capacity. At the optimum time, it attained 46 and 41.7 mg/g for NiONPs-CS and CuONPs-CS, respectively. The adsorption rate reached equilibrium after 60 min. A similar research trend was documented for the uptake of CIP on PAC@Fe₃O₄-MN[31] and the removal of ibuprofen using raw Cellulosic Sisal with polypyrrole−polypyrrole nanoparticles.[25]

Effect of CIP Concentration. The increase in the adsorbate concentration can positively affect the adsorption yield via enhancement of mass transfer. At lower adsorbate concentrations, more active sites are present to trap CIP, whereas at higher target drug concentrations, there are fewer available sites exhibiting decreased removal efficiency and increased adsorption capacity. As depicted in Figure 5e, with an increase in CIP concentration from 20 to 100 mg/L, the uptake capacity increased from 14.1 to 42.5, 15.7 to 63.3, and 16.0 to 67.3 mg/g for CS, NiONPs-CS, and CuONPs-CS. Greater interaction between the CIP drug and the functional groups at the surface site of the adsorbent is ascribed to the higher uptake of the antibiotic drug.[58] Again, a drastic decrease in percentage removal from 70.3 to 42.5, 78.3 to 63.3, and 80 to 67.3% for CS, NiONPs-CS, and CuONPs-CS was observed. At lower drug molecule concentrations, the active sites of the adsorbents could easily take up CIP contaminant from the aqueous medium but become saturated at higher molecule concentrations due to a limited number of active sites, thereby leaving behind some residual CIP in solution.[59,60]

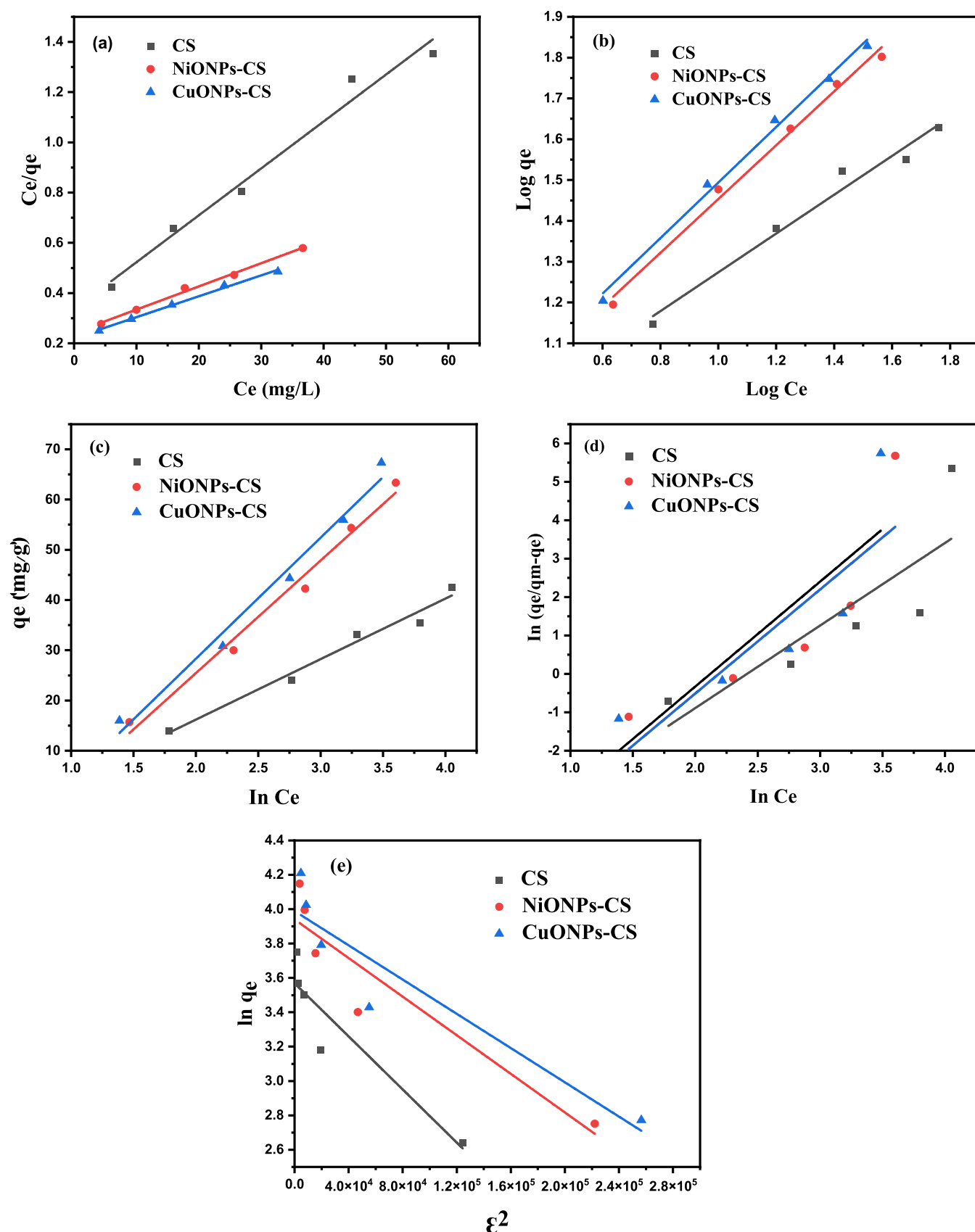**Figure 6.** (a) Langmuir, (b) Freundlich, (c) Temkin, (d) Sips, and (e) Dubinin−Radushkevich plots for CIP uptake onto CS, NiONPs-CS, and CuONPs-CS.

Effect of Temperature. Temperature is another important parameter as demonstrated in adsorption studies due to its

connection with thermodynamic studies, implying that the impact of temperature on the adsorptive potency of the raw

adsorbent and nanocomposite materials for CIP was examined at fixed optimum values of pH, dosage, concentrations, and time. Figure 5f shows the removal efficiency that increased from 60.4 to 65.8, 69.8 to 73.9, and 72.1 to 81.7% for CS, NiONPs-CS, and CuONPs-CS by raising the temperatures, thus depicting that the studied adsorbent interactions with CIP molecules were endothermic in nature and adsorption is favored at increased temperature. Biosorption efficiency is highly noticed in prepared nanocomposites compared to the raw sample as a result of creation of more adsorbing pore sites or expansion of the volume of inner pores for further interaction with the target pollutant;[61] again, a decrease in the viscosity of aqueous solution at increasing temperature can facilitate the movement of CIP particles toward the adsorbent surface sites, thus leading to a fast collision rate between the adsorbate molecules and the adsorbents.[62−64]

Isotherm Modeling. In order to understand the biosorption of CIP onto CS, NiONPs-CS, and CuONPs-CS, the equilibrium isotherm was carried out with antibiotic drug concentrations ranging from 20 to 100 mg/L at room temperature. Selected isotherm models such as Langmuir, Freundlich, Temkin, SiPs, and D−R isotherms[45,65] shown in Table 1 were used to elucidate the sorption features between the target pollutant and the prepared adsorbents. Additionally, standard error analyses were performed to obtain the most fitting isotherm model to describe the adsorption process. The isotherm models for fitting CIP onto prepared adsorbents are demonstrated in Figure 6, whereas Table 1 presents estimated model parameters. The Langmuir isotherm is based on monolayer and homogeneous distribution of surface sites for the target pollutant with equivalent energy on the adsorbent surface, whereas in the Freundlich isotherm, there is the existence of nonuniform and heterogeneous distribution of adsorption sites with different affinities.[66,67] The limiting behavior of Langmuir and Freundlich leads to a Sips isotherm. Temkin denotes a strong electrostatic interaction between the adsorbate and adsorbent.[67] The D−R model deals with the porous nature of the adsorbents and the energy of the adsorption process.[68] Based on the regression value, R^2, and error analyses, the Langmuir model gave the best fit for the adsorption of CIP onto raw and nanocomposite adsorbents, followed by Temkin and Freundlich isotherms. The monolayer adsorption capacity, q_{max}, of CIP drug on CS, NiONPs-CS, and CuONPs-CS were found to be 53.53, 108.34, and 120.19 mg/g, respectively, indicating the higher adsorption capacity of nickel and copper oxide impregnation onto CS for the CIP drug than raw corn silk. Although Freundlich and Temkin models gave good R^2 (0.9750, CS; 0.9927, NiONPs-CS; and 0.9939, CuONPs-CS and 0.9751, CS; 0.9843, NiONPs-CS and 0.9825, CuONPs-CS), higher error analyses showed that these models would not be fit to describe the uptake capacity of CIP onto prepared adsorbents. Sips and D−R isotherms gave lower fittings for the adsorption process owing to their reduced regression values and high statistical error values. Considering all scenarios, including higher regression values and monolayer capacities, it can be observed that the incorporated nano-adsorbents showed an increased adsorption process than the raw adsorbent (CuONPs-CS > NiONPs-CS > CS).

The comparison of the prepared CS, NiONPs-CS, and CuONPs-CS with other various adsorbents toward the monolayer adsorption capacity and fit isotherm model attributed to the CIP drug is presented in Table 2. For the removal of emergent pollutants, the adsorption performance of

Table 2. Comparative Adsorption Study of CIP Removal with Other Literature Studies

adsorbents	q_m (mg/g)	isotherm	references
CuO nanoparticles	89.46	Freundlich	69
Zinc oxide-impregnated activated carbon	15.75	Freundlich	70
ACAF/Fe$_3$O$_4$/ZnO	178.8	Freundlich	6
G. ghatti-cl-P(AAm)/NiFe$_2$O$_4$	274.84	Langmuir	27
AC loaded with Ni−Co−S nanoparticles	744.70	Temkin	28
Fe$_3$O$_4$/C	98.28	Langmuir	71
MgO nanoparticles	3.46	Langmuir	72
PAC@Fe$_3$O$_4$-MN	109.33	Langmuir	31
HNO$_3$-modified corn cob	51.55	Freundlich	15
raw corn cob	26.31	Freundlich	73
Cu-glutamate MOF	61.35	Langmuir	74
pistachio shell powder-coated ZnO nanoparticles	98.72	Freundlich	75
NiO nanoparticles	99.81	Freundlich	76
graphene oxide/sodium alginate	86.12	Langmuir	77
chitosan/kaolin/Fe$_3$O$_4$	47.85	Langmuir	78
carbon nanofibers	10.36	Langmuir	79
bentonite−chitosan nanocomposite	39.06	Langmuir	80
CS	53.53	Langmuir	this study
NiONPs-CS	108.34	Langmuir	this study
CuONPs-CS	120.19	Langmuir	this study

the studied adsorbents showed good efficiency in comparison with previous studies (Table 2). The adsorption of the prepared nanocomposites was relatively higher than those of CuO nanoparticles (89.46 mg/g),[69] ZnO-impregnated activated carbon (15.75 mg/g),[70] and iron oxide-loaded carbon (98.28 mg/g).[71] Notably, prepared adsorbents were able to adsorb the cationic and anionic parts of the CIP drug, making them potential adsorbents for industrial applications.

Kinetic Evaluation. Kinetic studies provide information on whether adsorption takes place via mass transfer, diffusion, or chemical reactions. This study explains the uptake of the CIP adsorbate onto investigated adsorbents, which successively controls the time taken by the adsorbate at the boundary between the adsorbent and the bulk solution. To further elaborate on the aforementioned statements, the adsorption efficiency of the CIP drug onto CS, NiONPs-CS, and CuONPs-CS data was analyzed by pseudo-first-order, pseudo-second-order, Elovich, intraparticle diffusion, and liquid film diffusion kinetic models.[15,81,82] The plots of the linearized form of the selected kinetics at different time ranges are shown in Figure 7A−E. The rate constants determined from the plots together with the corresponding regression coefficient and other parameters at 298 K are presented in Table 3. The suitability of the kinetic model is based on the regression coefficient (R^2) and error function. In the case of the PFO model, R^2 values were 0.8212, 0.9261, and 0.9047; however, for the PSO model, they were 0.9142, 0.9861, and 0.9991, and the Elovich model gave R^2 values of 0.8316, 0.8599, and 0.8061 for CS, NiONPs-CS, and CuONPs-CS, respectively. The calculated coefficient values that are close to unity reveal that the PSO assumption is appropriate for CIP adsorption by raw corn silk, nickel oxide, and copper oxide nanoparticle-loaded corn silk with a lower residual sum of square (RSS) error coefficient than other kinetic models. The above findings suggest adsorption by the chemical process, and
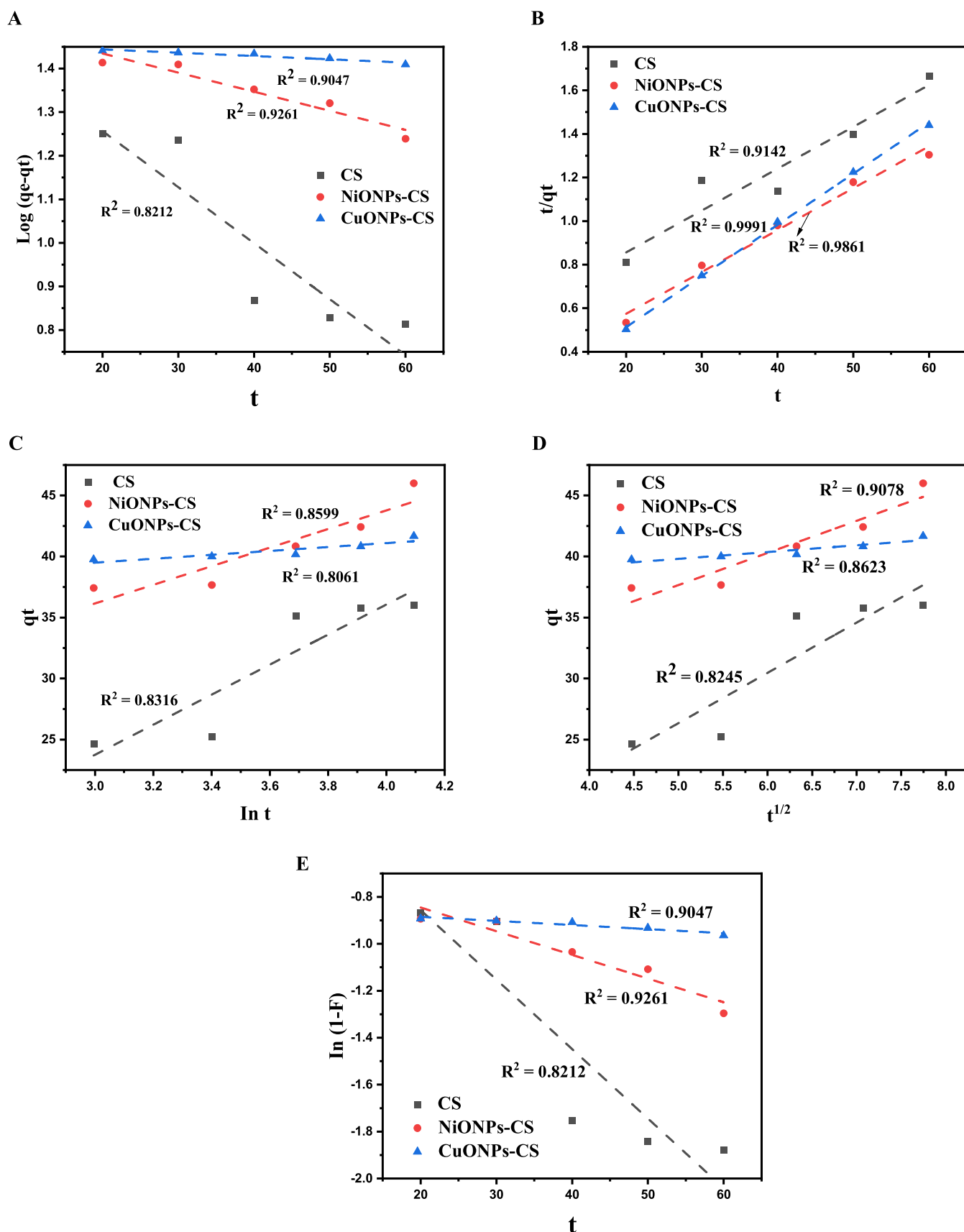
Figure 7. (A) Pseudo-first-order, (B) pseudo-second-order, (C) Elovich, (D) intraparticle diffusion, and (E) liquid film diffusion plots for CIP uptake onto CS, NiONPs-CS, and CuONPs-CS.

Table 3. Kinetic Parameters for the Adsorption of CIP on CS, NiONPs-CS, and CuONPs-CS

models	parameters	CS	NiONPs-CS	CuONPs-CS
Pseudo-first-order	$q_{e,exp}$ (mg/g)	36.00	46.00	41.67
$\log(q_e - q_t) = \log q_e - \dfrac{K_1 t}{2.303}$	k_1 (min^{-1})	0.030	0.010	0.002
q_e = adsorption capacity at equilibrium time and q_t = adsorption capacity at time t (mg/g), k_1 (1/min) = equilibrium rate constant for pseudo-first-order	$q_{e,calcd}$ (mg/g)	32.63	33.28	28.78
	R^2	0.8212	0.9261	0.9047
	RSS	0.036	0.002	6.08×10^{-5}
Pseudo-second-order	k_2 (mg/g·min)	0.001	0.002	0.013
$\dfrac{t}{q_t} = \dfrac{1}{k_2 q_e{}^2} + \dfrac{t}{q_e}$	$q_{e,calcd}$	52.06	52.03	42.58
k_2 (g/mg min) = equilibrium rate constant for pseudo-second-order	R^2	0.9142	0.9861	0.9991
	RSS	0.035	0.005	0.001
Elovich	α (g·min^2/mg)	4.22	43.47	29.86
$q_t = \dfrac{1}{\beta}\ln(\alpha\beta) + \dfrac{1}{\beta}\ln(t)$	β (g·min/mg)	0.08	0.13	0.62
q_t = amount of the adsorbate/g adsorbent at time (t), α is the initial adsorption rate (mg/g min); β is the desorption constant (g/mg) during any one experiment	R^2	0.8316	0.8599	0.8061
	RSS	23.125	7.131	0.4643
Intraparticle diffusion	K_{id} (mg/g/min$^{1/2}$)	4.12	2.63	0.56
$q_t = K_{id}t^{1/2} + C$	C	5.75	24.50	37.02
q_t = amount of the adsorbate/g adsorbent at time (t), K_{id} (mg/g/min$^{1/2}$) is the equilibrium rate constants of intraparticle diffusion adsorption; C corresponds to the intercept of the IPD equation	R^2	0.8245	0.9078	0.8623
	RSS	24.099	4.692	0.330
Liquid film diffusion	K_{fd}	0.029	0.010	0.002
$\ln(1-F) = -K_{LFD}t + C$	C	−0.264	−0.643	−0.850
$F = \dfrac{[q_t]}{[q_e]}$	R^2	0.8212	0.9261	0.9047
K_{LFD} (min^{-1}) is the equilibrium rate constant of liquid film diffusion adsorption; C corresponds to the intercept of the LFD equation. Constant F represents the fractional attainment of equilibrium	RSS	0.191	0.008	3.22×10^{-4}

there was no resistance during internal diffusion of the adsorbate ion.[83] Furthermore, the experimental q_e agrees with the computational q_e, and the values are quite close to each other except for raw corn silk, thus indicating the consistency of the data with the model and that the adsorbents are saturated and have reached equilibrium. This also depicts that NiONPs-CS and CuONPs-CS nanocomposites are better adsorbing materials to remove CIP contaminants than raw corn silk following the kinetic model evaluation.

The kinetic parameters were also determined by intraparticle diffusion (IPD) and liquid film diffusion (LFD) models. These models play essential roles in the diffusion mechanism in adsorption kinetics. Table 3 shows the coefficients of both models. For IPD, the linear regression coefficient was higher than 0.900 for only NiONPs-CS nanosorbent, whereas for LFD, NiONPs-CS and CuONPs-CS nanocomposites recorded regression values above 0.900 with no zero intercepts, as the linear diagram of IPD and LFD did not pass through the origin, which indicates the involvement of boundary layer thickness during the adsorption process.[84] Thus, neither the IPD nor LFD model is the only rate-controlling step; rather, other possible diffusion mechanisms are involved. Similar findings were reported on sorption of chlorpyrifos onto ZnONP-impregnated pea peels,[42] adsorptive removal of paracetamol onto biosynthesized CuO nanoparticles,[39] and CIP adsorption onto ZnO nanoparticle-loaded activated carbon derived from *Azolla filiculoides* biomass.[6]

Thermodynamics. Thermodynamic properties can be utilized to ascertain information on the adsorption of CIP onto CS, NiONPs-CS, and CuONPs-CS and their mechanisms. For a better understanding of the spontaneity of the adsorption process of the CIP drug onto CS, NiONPs-CS, and CuONPs-CS, the Gibbs free energy was estimated according to eq 7.[85] The determination of enthalpy and entropy was made possible from the van't Hoff diagram using the slope and intercept of the plot, as shown in Figure 8.
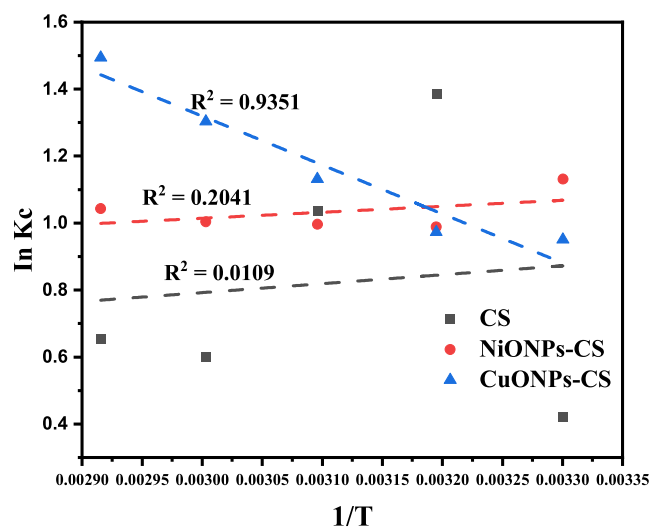

Figure 8. Van't Hoff plot for the adsorptive removal of CIP by CS, NiONPs-CS, and CuONPs-CS.

The following equations were used for the thermodynamic study[86,87]

$$\Delta G^\circ = -RT \ln K_C = \Delta H^\circ - T\Delta S^\circ \qquad (7)$$

$$\ln K_C = -\left(\frac{\Delta H^\circ}{RT}\right) + \left(\frac{\Delta S^\circ}{R}\right) \qquad (8)$$

$$\ln K_C = \frac{q_e}{c_e} \qquad (9)$$

Table 4. Thermodynamic Analysis of CIP Adsorption onto CS, NiONPs-CS, and CuONPs-CS

adsorbents	temperature (K)	$\Delta G°$ (kJ/mol)	$\Delta H°$ (kJ/mol)	$\Delta S°$ (J/mol·K)	R^2
CS	303	−2.198	−2.218	−0.066	0.0109
	313	−2.197			
	323	−2.197			
	333	−2.196			
	343	−2.195			
NiONPs-CS	303	−2.690	−1.492	3.96	0.2041
	313	−2.730			
	323	−2.769			
	333	−2.809			
	343	−2.848			
CuONPs-CS	303	−2.218	12.138	47.38	0.9351
	313	−2.692			
	323	−3.166			
	333	−3.640			
	343	−4.113			

where $\Delta G°$ is the change in standard Gibbs free energy, R is a universal gas constant 8.314 J/(mol. K), T = temperature, $\Delta H°$, $\Delta G°$, and $\Delta S°$ denotes change in enthalpy, free energy, and entropy, respectively, and K_C is the adsorption thermodynamic equilibrium constant.

The negative $\Delta G°$ values at temperatures of 30, 40, 50, 60, and 70 °C showed that the adsorption of CIP onto the studied adsorbents occurs spontaneously and thermodynamically favorably at higher temperatures, as shown in Table 4. Additionally, it was observed that impregnation of corn silk with nickel and copper oxide nanoparticles increased the spontaneity of the adsorption process for all of the studied temperatures when compared with CS.

The nature of the exothermic process was confirmed by the negative values of $\Delta H°$ for CS and NiONPs-CS, whereas the endothermic reaction process was ascertained by the positive value of $\Delta H°$ for the CuONPs-CS adsorbent. The adsorption phenomenon can be described as the physisorption-controlled mechanism, since the enthalpy values are lower than 40 kJ/mol.[88] The negative value of $\Delta S°$ as presented by CS indicates accumulation of CIP molecules on the adsorbent surface in ordered layers, whereas for NiONPs-CS and CuONPs-CS, the positive entropy values showed an increase in randomness during the adsorption of CIP at the liquid−solid interface. The increased adsorption capacity at higher temperatures for CuONP-loaded adsorbents has been reported to be due to pore size enlargement and surface activation.[39]

Recyclability. With regard to cost-effectiveness and environmental impact, the stability and recycle period of an adsorbent are essential factors in evaluating the practical application of the tested nanocomposites. The stability and recyclability of CS, NiONPs-CS, and CuONPs-CS were investigated, as presented in Figure 9. It can be seen from the first cycle that 74.6, 82.8, and 83.7% of CIP removal were observed for CS, NiONPs-CS, and CuONPs-CS, respectively. These results validate the stability and durability of the studied adsorbents for repeated reuse in the uptake of CIP antibiotics from wastewater and are compared favorably with the adsorption of heavy metals from wastewater by corn cob and coconut husk.[89] Nevertheless, 47.8, 63.1, and 66.9% were observed after five adsorption cycles. This decrease in performance could be ascribed to the weight loss of the adsorbent materials, saturation of the pores, and the effect of the repeated treatment during the elution process, resulting in
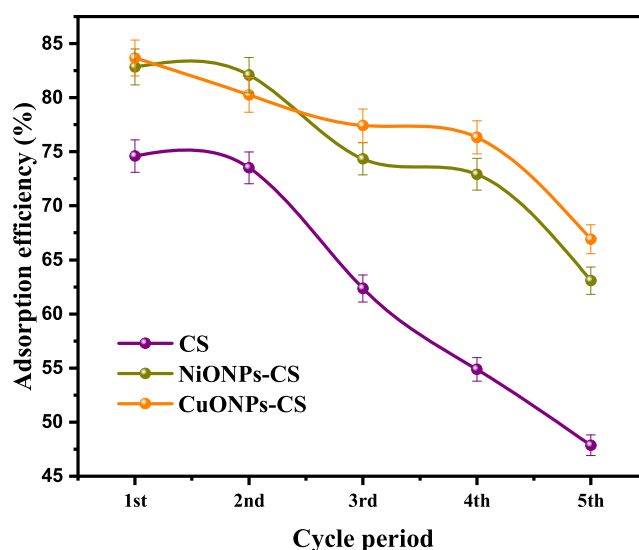

Figure 9. Effect of reusability on the removal of CIP on CS, NiONPs-CS, and CuONPs-CS.

the loss of active binding sites on the adsorbing materials.[90] However, the nanoparticle-loaded adsorbents portrayed effective potential for recycling irrespective of the aforementioned factors. Additionally, the spent adsorbents produced after extensive reuse can be used as additives in building material production to increase the compressive strength.[24] Over 75% of methylene blue removal efficiency was recorded by Pei et al.[91] even after 10 adsorption/desorption cycles using 0.1 M HCl/ethanol solutions (20 mL) as an eluent, which proved the effectiveness of regeneration and recycling of the newly fabricated porous hydrogel bead-like sorbent.

Adsorption Mechanism. An understanding of the sorption interaction between the studied adsorbents and CIP drug is crucial in the adsorption process mechanism. The elucidation from the FTIR analysis of the adsorbents before and after CIP adsorption provided an insight into the mechanism of CIP adsorption onto CS, NiONPs-CS, and CuONPs-CS. This is important as shift in the adsorption band of the adsorbing materials helps to note the vibrational functional groups responsible for adsorption of the CIP antibiotic.[92] The depicted FTIR spectra (Figure 1d) of CS, NiONPs-CS, and CuONPs-CS before and after CIP

adsorption showed that O−H, C=O, and C−O were responsible for the uptake of CIP onto the adsorbents. It has been stated that the presence of O−H, N−H, and C=O functional moieties on the biosorbent shows the good uptake of the pollutant from aqueous solution.[93] The impregnation of NiO and CuO nanoparticles actually improved the active surface sites of the nanosorbents. The adsorptive removal of CIP from wastewater occurred through hydrogen bonding, pi−pi, electrostatic, and hydrophobic interactions based on the involvement of hydroxyl and carboxyl functional groups.[94,95] It may be proposed that the carboxylic acid groups in CIP interact by complexation with nickel and copper oxide surface groups, which can occur by bidentate or bridged bidentate complexes.[96] Again, based on kinetic tests and adsorption isotherms performed, it can be proposed that physisorption interaction occurs by electrostatic attraction.[88] In addition to the confirmation of the existing electrostatic interaction being the primary adsorption mechanism for the removal of CIP from wastewater, the influence of solution pH was involved. An increase in pH above the point of zero charge of NiONPs-CS and CuONPs-CS increased the adsorption capacity and removal of CIP. A further increase in pH possibly enhanced the adsorption capacity of CIP due to deprotonation of the adsorbent surface that promotes the electrostatic attraction between the CIP antibiotic and negatively charged NiONPs-CS and CuONPs-CS surfaces. For porous adsorbent materials, pore filling is also a typical mechanism that occurs, allowing for improved uptake. Qin et al.[97] reported adsorption (chemisorption and physical adsorption) and pore filling as the main adsorption mechanisms of p-nitrophenol on biochar. This is possible because multiple layers of CIP are required, and the data fit well to the Freundlich model for multilayer uptake. The adsorption mechanism is summarized in Figure 10.
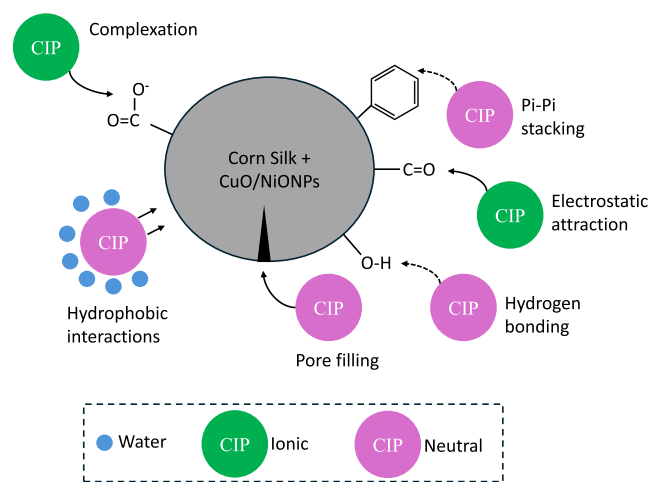

Figure 10. Summary of the CIP adsorption mechanism toward NiONPs-CS and CuONPs-CS.

CONCLUSIONS

Biobased corn silk incorporating nickel oxide and copper oxide was fabricated for the removal of the CIP drug from wastewater. The functional group, crystallographic, morphological, and N_2 adsorption−desorption characteristics were determined. A comparative evaluation of the potential of CS, NiONPs-CS, and CuONPs-CS on the uptake of CIP depicted the higher adsorption efficiency of nanocomposites, most especially CuONPs-CS, than the raw biomass. Different varying parameters, such as solution pH, contact time, dosage, temperature, and initial CIP concentration, were investigated to ascertain their impacts on the adsorptive removal of CIP by NiONPs-CS and CuONPs-CS. The analyzed results showed that increasing the dose, contact time, pH, and temperature of the nanocomposites increased the removal percentage of the pollutant. On the contrary, with the increase in the initial CIP concentration, there is a reduction in percentage removal. The Langmuir isotherm demonstrated a strong fit for the generated CIP equilibrium data with monolayer adsorption capacities of 108.34 mg/g for NiONPs-CS and 120.19 mg/g for CuONPs-CS at 303 K. The best fit was further confirmed by lower calculated statistical error values. The pseudo-second-order kinetic model accurately matched the experimental data for the nanosorbents attaining equilibrium at 60 min. The adsorption process was spontaneously favorable and exothermic for NiONPs-CS and endothermic for CuONPs-CS based on thermodynamic evaluation. The nanocomposites exhibited reliable reusability for five repeated adsorption cycles. Thus, the developed NiONPs-CS and CuONPs-CS nanocomposites exhibited excellent adsorption performance with high adsorption capacity and promising capability to remove CIP from polluted water.

AUTHOR INFORMATION

Corresponding Author

Chisom Theresa Umeh − *Environmental Chemistry and Toxicology Research Unit, Pure and Industrial Chemistry Department, Nnamdi Azikiwe University, P.M.B., Awka 5025 Anambra, Nigeria;* orcid.org/0000-0001-8161-6517; Email: umehchi871@gmail.com, uc.umeh@unizik.edu.ng

Authors

John Kanayochukwu Nduka − *Environmental Chemistry and Toxicology Research Unit, Pure and Industrial Chemistry Department, Nnamdi Azikiwe University, P.M.B., Awka 5025 Anambra, Nigeria*

Kovo Godfrey Akpomie − *Department of Pure & Industrial Chemistry, University of Nigeria, Nsukka 410002, Nigeria; Department of Chemistry, University of the Free State, Bloemfontein 9300, South Africa;* orcid.org/0000-0003-2986-4294

Joshua O. Ighalo − *Department of Chemical Engineering, Nnamdi Azikiwe University, P.M.B., Awka 5025, Nigeria;* orcid.org/0000-0002-8709-100X

Refilwe Mogale − *Department of Chemistry, University of the Free State, Bloemfontein 9300, South Africa*

Complete contact information is available at:
https://pubs.acs.org/10.1021/acsomega.4c09192

projects (RP) intervention fund [TETF/ES/DR&D/CE/UNI/AWKA/IRR/2023/VOL.1] to conduct this research.

■ REFERENCES

(1) Mohammed, N.; Grishkewich, N.; Tam, K. C. Cellulose Nanomaterials: Promising Sustainable Nanomaterials for Application in Water/Wastewater Treatment Processes. *Environ. Sci.: Nano* 2018, 5, 623.

(2) Mahshid, M.; Maryam, F.; Mohammad, M.; Majid, N. Ciprofloxacin removal from aqueous media by adsorption process: a systematic review and meta-analysis. *Desalin. Water Treat.* 2021.

(3) Carabineiro, S. A. C.; Thavorn-amornsri, T.; Pereira, M. F. R.; Serp, P.; Figueiredo, J. L. Comparison between activated carbon, carbon xerogel and carbon nanotubes for the adsorption of the antibiotic ciprofloxacin. *Catal. Today* 2012, 186, 29−34.

(4) Carabineiro, S. A. C.; Thavorn-Amornsri, T.; Pereira, M. F. R.; Figueiredo, J. L. Adsorption of ciprofloxacin on surface-modified carbon materials. *Water Res.* 2011, 45, 4583−4591.

(5) Jin, J. H.; Yang, Z. H.; Xiong, W. P.; Zhou, Y. Y.; Xu, R.; Zhang, Y. R.; Cao, J.; Li, X.; Zhou, C. Y. Cu and Co nanoparticles co-doped MIL-101 as a novel adsorbent for efficient removal of tetracycline from aqueous solutions. *Sci. Total Environ.* 2019, 650, 408−418.

(6) Alameri, A. A.; Alfilh, R. H. C.; Awad, S. A.; Zaman, G. S.; Al-Musawi, T. J.; Joybari, M. M.; Balarak, D.; McKay, G. Ciprofloxacin adsorption using magnetic and ZnO nanoparticles supported activated carbon derived from *Azolla filiculoides* biomass. *Biomass Convers. Biorefin.* 2024, 14, 27001.

(7) Malakootian, M.; Ahmadian, M. Ciprofloxacin removal by electro-activated persulfate in aqueous solution using iron electrodes. *Appl. Water Sci.* 2019, 9, 2−10.

(8) Amirmahani, N.; Mahdizadeh, H.; Malakootian, M.; Pardakhty, A.; Mahmoodi, N. O. Evaluating nanoparticles decorated on $Fe_3O_4@SiO_2$-schiff base ($Fe_3O_4@SiO_2$-APTMS-HBA) in adsorption of ciprofloxacin from aqueous environments. *J. Inorg. Organomet. Polym. Mater.* 2020, 30, 1−12.

(9) Zhu, X.; Tsang, D. C. W.; Chen, F.; Li, S.; Yang, X. Ciprofloxacin adsorption on graphene and granular activated carbon: kinetics, isotherms, and effects of solution chemistry. *Environ. Technol.* 2015, 36, 3094−3102.

(10) Balarak, D.; Mahvi, A. H.; Shim, M. J.; Lee, S.-M. Adsorption of ciprofloxacin from aqueous solution onto synthesized NiO: isotherm, kinetic and thermodynamic studies. *Desalin. Water Treat.* 2020, 203, 1−11.

(11) Dehghani, M.; Nozari, M.; A Fakhraei Fard, A.; M Ansari Shiri, M.; N Shamsedini, N. Direct red 81 adsorption on iron filings from aqueous solutions; kinetic and isotherm studies. *Environ. Technol.* 2019, 40, 1705−1713.

(12) Kumar, A.; Patra, C.; Kumar, S.; Narayanasamy, S. Effect of magnetization on the adsorptive removal of an emerging contaminant ciprofloxacin by magnetic acid activated carbon. *Environ. Res.* 2022, 206, No. 112604.

(13) Giahi, M.; Rahbar, A.; Mehdizadeh, K. Photochemical degradation of an environmental pollutant by pure ZnO and MgO doped ZnO nanocatalysts. *Iran. J. Chem. Chem. Eng.* 2021, 40 (1), 83−91.

(14) Lakshman, M. $Fe_3O_4@SiO_2$-Pip-SA nanocomposite: a novel and highly efficient reusable acidic catalyst for synthesis of rhodanine derivatives. *J. Synth. Chem.* 2022, 1 (1), 48−51.

(15) Umeh, C. T.; Nduka, J. K.; Iwuozor, K. O.; Omokpariola, O. D.; Dulta, K.; Ezeh, S. C.; Emeka, R. N. Adsorption modelling on the removal of ciprofloxacin antibiotic from aqueous solution by acid-modified corn cob. *Int. J. Environ. Anal. Chem.* 2023, 1−26.

(16) Ezekoye, O. M.; Akpomie, K. G.; Eze, S. I.; Chukwujindu, C. N.; Ani, J. U.; Ujam, O. T. Biosorptive interaction of alkaline modified Dialium guineense seed powders with ciprofloxacin in contaminated solution: central composite, kinetics, isotherm, thermodynamics, and desorption. *Int. J. Phytorem.* 2020, 22, 1−10.

(17) Sassa-deepaeng, T.; Yodthong, W.; Khumpirapang, N.; Anuchapreeda, S.; Okonogi, S. Effects of plant-based copper nanoparticles on the elimination of ciprofloxacin. *Drug Discov. Ther.* 2023, 17, 320.

(18) Khan, S. A.; Ismail, M.; Anwar, Y.; Farooq, A.; Al Johny, B. O.; Akhtar, K.; Shah, Z. A.; Nadeem, M.; Raza, M. A.; Asiri, A. M.; Khan, S. B. A highly efficient and multifunctional biomass supporting Ag, Ni, and Cu nanoparticles through wetness impregnation for environmental remediation. *Green Process Synth.* 2019, 8, 309−319.

(19) Krishnaraj, C.; Jagan, E.; Rajasekar, S.; Selvakumar, P.; Kalaichelvan, P.; Mohan, N. Synthesis of silver nanoparticles using Acalypha indica leaf extracts and its antibacterial activity against water borne pathogens. *Colloids Surf., B* 2010, 76, 50−56.

(20) Eid, A. M.; Fouda, A.; Hassan, S. E.-D.; Hamza, M. F.; Alharbi, N. K.; Elkelish, A.; Alharthi, A.; Salem, W. M. Plant-Based Copper Oxide Nanoparticles; Biosynthesis, Characterization, Antibacterial Activity, Tanning Wastewater Treatment, and Heavy Metals Sorption. *Catalysts* 2023, 13, 348.

(21) Hamza, M. F.; Abdel-Rahman, A. A. H.; Hawata, M. A.; El Araby, R.; Guibal, E.; Fouda, A.; Wei, Y.; Hamad, N. A. Functionalization of magnetic chitosan microparticles—Comparison of trione and trithione grafting for enhanced silver sorption and application to metal recovery from waste X-ray photographic films. *J. Environ. Chem. Eng.* 2022, 10, No. 107939.

(22) Bhatnagar, A.; Hogland, W.; Marques, M.; Sillanpaa, M. An overview of the modification methods of activated carbon for its water treatment applications. *Chem. Eng. J.* 2013, 219, 499−511.

(23) Osagie, C.; Othmani, A.; Ghosh, S.; Malloum, A.; KashitarashEsfahani, Z.; Ahmadi, S. Dyes adsorption from aqueous media through the nanotechnology: A review. *J. Mater. Res. Technol.* 2021, 14, 2195.

(24) Akpomie, K. G.; Conradie, J. Efficient synthesis of magnetic nanoparticle-*Musa acuminata* peel composite for the adsorption of anionic dye. *Arabian J. Chem.* 2020, 13, 7115−7131.

(25) Khadir, A.; Motamedi, M.; Negarestani, M.; Sillanpää, M.; Sasani, M. Preparation of a nano bio-composite based on cellulosic biomass and conducting polymeric nanoparticles for ibuprofen removal: Kinetics, isotherms, and energy site distribution. *Int. J. Biol. Macromol.* 2020, 162, 663.

(26) Prajapati, A. K.; Mondal, M. K. Comprehensive kinetic and mass transfer modeling for methylene blue dye adsorption onto CuO nanoparticles loaded on nanoporous activated carbon prepared from waste coconut shell. *J. Mol. Liq.* 2020, 307, 112949.

(27) Gor, A. H.; Dave, P. N. Adsorptive abatement of ciprofloxacin using $NiFe_2O_4$ nanoparticles incorporated into G. ghatti-cl-P(AAm) nanocomposites hydrogel: isotherm, kinetic, and thermodynamic studies. *Polymer Bulletin* 2019, 77, 5589−5613.

(28) Chowdhury, A.; Kumari, S.; Khan, A. A.; Chandra, M. R.; Hussain, S. Activated carbon loaded with Ni-Co-S nanoparticle for Superior Adsorption Capacity of Antibiotics and Dye from Wastewater: Kinetics and Isotherms. *Colloids Surf., A* 2021, 611, 125868.

(29) Gupta, V. K.; Arunima Nayak, A. Cadmium removal and recovery from aqueous solutions by novel adsorbents prepared from orange peel and Fe_2O_3 nanoparticles. *Chem. Eng. J.* 2012, 180, 81−90.

(30) Chen, L.; Ji, T.; Mu, L.; Shi, Y.; Brisbin, L.; Guo, Z.; Khan, M. A.; Young, D. P.; Zhu, J. Facile Synthesis of Mesoporous Carbon Nanocomposites from Natural Biomass for Efficient Dye Adsorption and Selective Heavy Metal Removal. *RSC Adv.* 2016, 6, No. 2259.

(31) Al-Musawi, T. J.; Mahvi, A. H.; Khatibi, A. D.; Balarak, D. Effective adsorption of ciprofloxacin antibiotic using powdered activated carbon magnetized by iron (III) oxide magnetic nanoparticles. *J. Porous Mater.* 2021, 28, 835−852.

(32) Dai, Q.; Yuan, B.; Guo, M.; Zhang, K.; Chen, X.; Song, Z.; Nguyen, T. T.; Wang, X.; Lin, S.; Fan, J.; Li, Y.; Liu, H.; Guo, Z. A novel nano-fibriform C- modified niobium pentoxide by using cellulose templates with highly visible-light photocatalytic performance. *Ceram. Int.* 2020, 46, 13210−13218.

(33) Fu, Q.; Cao, H.; Liang, G.; Luo, L.; Chen, Y.; Murugadoss, V.; Wu, S.; Ding, T.; Lin, C.; Guo, Z. A highly Li^+-conductive $HfNb_{24}O_{62}$ anode material for superior Li^+ storage. *Chem. Commun.* 2020, 56, 619−622.

(34) Kaur, D.; Bagga, V.; Behera, N.; Thakral, B.; Asija, A.; Kaur, J.; Kaur, S. SnSe/SnO$_2$ nanocomposites: novel material for photocatalytic degradation of industrial waste dyes. *Adv. Compos. Hybrid Mater.* **2019**, *2*, 763−776.

(35) Ghaedi, M.; Sadeghian, B.; Amiri Pebdani, A.; et al. Kinetics, thermodynamics and equilibrium evaluation of direct yellow 12 removal by adsorption onto silver nanoparticles loaded activated carbon. *Chem. Eng. J.* **2012**, *187*, 133−141.

(36) Du, Y.; Dai, M.; Cao, J.; Peng, C.; Ali, I.; Naz, I.; Li, J. Efficient removal of acid orange 7 using a porous adsorbent supported zerovalent iron as a synergistic catalyst in advanced oxidation process. *Chemosphere* **2020**, *244*, No. 125522.

(37) Li, N.; Zhang, F.; Wang, H.; Hou, S. Catalytic Degradation of 4-Nitrophenol in Polluted Water by Three-Dimensional Gold Nanoparticles/Reduced Graphene Oxide Microspheres. *Eng. Sci.* **2019**, *7*, 72−79.

(38) Anand, G. T.; Nithiyavathia, R.; Ramesha, R.; Sundarama, S. J.; Kaviyarasu, K. Structural and optical properties of nickel oxide nanoparticles: Investigation of antimicrobial applications. *Surf. Interfaces* **2020**, *18*, No. 100460.

(39) Akpomie, K. G.; Conradie, J. Efficient adsorptive removal of paracetamol and thiazolyl blue from polluted water onto biosynthesized copper oxide nanoparticles. *Sci. Rep.* **2023**, *13*, No. 859.

(40) Mohamed, S.; Alsaihi, S. Microwave-assisted synthesis of Nickel oxide nanoparticles using Coriandrum Sativum leaf extract and their structural-magnetic catalytic properties. *Materials* **2017**, *10*, 460.

(41) Rather, M. Y.; Sundarapandian, S. Facile green synthesis of copper oxide nanoparticles and their rhodamine-b dye adsorption property. *J. Cluster Sci.* **2022**, *33*, 925−933.

(42) Haq, Au.; Saeed, M.; Usman, M.; Naqvi, S. A. R.; Bokhari, T. H.; Maqbool, T.; Ghaus, H.; Tahir, T.; Khalid, H. Sorption of chlorpyrifos onto Zinc Oxide nanoparticles impregnated Pea peels (Pisum sativum L): Equilibrium, kinetic and thermodynamic studies. *Environ. Technol. Innov.* **2019**, *17*, No. 100516.

(43) Kalantar, Z.; Nasab, S. G. Modeling and optimizing Cd(II) ions adsorption onto Corn Silk/Zeolite-Y composite from industrial effluents applying response surface methodology: isotherm, kinetic, and reusability studies. *J. Iran. Chem. Soc.* **2022**, *19*, 4209−4221.

(44) Petroviᶜc, M.; Šoštariᶜc, T.; Stojanovic, M.; Petroviᶜc, J.; Mihajloviᶜc, M.; Ćosoviᶜc, A.; Stankoviᶜc, S. Mechanism of adsorption of Cu^{2+} and Zn^{2+} on the cornsilk (Zea mays L.) Ecological. *Engineering* **2017**, *99*, 83−90.

(45) Umeh, C. T.; John, K. N.; Refilwe, M.; Kovo, G. A.; Nkechi, H. O. Acid activated corn silk as a promising phytosorbent for uptake of malachite green and Cd (II) ion from simulated wastewater: Equilibrium, kinetic and thermodynamic studies. *Int. J. Phytorem.* **2024**, *26* (10), 1593−1610.

(46) Alhalili, Z. Green synthesis of copper oxide nanoparticles CuO NPs from Eucalyptus globoulus leaf extract: Adsorption and design of experiments. *Arab. J. Chem.* **2022**, *15*, No. 103739.

(47) Al-Qasmi, N. Facial Eco-Friendly Synthesis of Copper Oxide Nanoparticles Using Chia Seeds Extract and Evaluation of Its Electrochemical Activity. *Processes* **2021**, *9*, 2027.

(48) Eze, S. I.; Akpomie, K. G.; Ezeofor, C. C.; Osunkunle, A. A.; Maduekwe, O. B.; Okenyeka, O. U. Isotherm and Kinetic Evaluation of Dialium guineense Seed Husk and Its Modified Derivative as Efficient Sorbent for Crude Oil Polluted Water Treatment. *Water Conserv. Sci. Eng.* **2019**, *4*, 21−31.

(49) Jiang, W.; Zhang, L.; Guo, X.; Yang, M.; Lu, Y.; Wang, Y.; Zheng, Y.; Wei, G. Adsorption of cationic dye from water using an iron oxide/activated carbon magnetic composites prepared from sugarcane bagasse by microwave method. *Environ. Technol.* **2019**, *42*, 337−350.

(50) Chowdhury, R.; Khan, A.; Rashid, M. H. Green synthesis of CuO nanoparticles using Lantana camara flower extract and their potential catalytic activity towards the aza-Michael reaction. *RSC Adv.* **2020**, *10*, 14374−14385.

(51) Faisal, S.; Al-Radadi, N. S.; Jan, H.; Abdullah; Shah, S. A.; Shah, S.; Rizwan, M.; Afsheen, Z.; Hussain, Z.; Uddin, M. N.; Idrees, M.; Nadia Bibiet, N. Curcuma longa Mediated Synthesis of Copper Oxide, Nickel Oxide and Cu-Ni Bimetallic Hybrid Nanoparticles: Characterization and Evaluation for Antimicrobial, Anti-Parasitic and Cytotoxic Potentials. *Coatings* **2021**, *11*, 849.

(52) Guo, J.-Z.; Li, B.; Liu, L.; Lv, K. Removal of methylene blue from aqueous solutions by chemically modified bamboo. *Chemosphere* **2014**, *111*, 225−231.

(53) Polesel, F.; Plósz, B. G.; Trapp, S.; Andersen, H. R. *Modelling the Fate of Xenobiotic Trace Chemicals via Wastewater Treatment and Agricultural Resource Reuse*; Kgs. Lyngby: Technical University of Denmark, DTU Environment, 2016.

(54) Rahdar, A.; Rahdar, S.; Ahmadi, S.; Fu, J. Adsorption of ciprofloxacin from aqueous environment by using synthesized nanoceria. *Ecol. Chem. Eng. S* **2019**, *26* (2), 299−311.

(55) Dhiman, N.; Sharma, N. Batch adsorption studies on the removal of ciprofloxacin hydrochloride from aqueous solution using ZnO nanoparticles and groundnut (Arachis hypogaea) shell powder: a comparison. *Indian Chem. Eng.* **2019**, *61* (1), 67−76.

(56) Sousa, W. R. D. N.; Oliveira, A. R.; Filho, J. F. C.; Dantas, T. C. M.; Santos, A. G. D.; Caldeira, V. P. S.; Geraldo, E. L. Ciprofloxacin adsorption on ZnO supported on SBA-15. *Water, Air, Soil Pollut.* **2018**, *229*, 1−12.

(57) Li, C.; Chen, D.; Ding, J.; Shi, Z. A novel heteroexopolysaccharide for the adsorption of methylene blue from aqueous solutions: Isotherm, kinetic, and mechanism studies. *J. Cleaner Prod.* **2020**, *265*, No. 121800.

(58) Dehmani, Y.; Alrashdi, A. A.; Lgaz, H.; Lamhasni, T.; Abouarnadasse, S.; Chung, I.-M. Removal of phenol from aqueous solution by adsorption onto hematite (a-Fe$_2$O$_3$): Mechanism exploration from both experimental and theoretical studies. *Arab. J. Chem.* **2020**, *13* (5), 5474−5486.

(59) Khodadadi, M.; Al-Musawi, T. J.; Kamranifar, M.; Saghi, M. H.; Hossein Panahi, A. A comparative study of using barberry stem powder and ash as adsorbents for adsorption of humic acid. *Environ. Sci. Pollut. Res.* **2019**, *26* (25), 26159−26169.

(60) Zhang, L.; Song, X.; Liu, X.; Yang, L.; Pan, F.; Lv, J. Studies on the removal of tetracycline by multi-walled carbon nanotubes. *Chem. Eng. J.* **2011**, *178*, 26−33.

(61) Zhao, S.-X.; Ta, N.; Wang, X.-D. Effect of temperature on the structural and physicochemical properties of biochar with apple tree branches as feedstock material. *Energies* **2017**, *10* (9), 1293.

(62) Gao, Y.; Li, Y.; Zhang, L.; Huang, H.; Hu, J.; Shah, S. M.; Su, X. Adsorption and removal of tetracycline antibiotics from aqueous solution by graphene oxide. *J. Colloid Interface Sci.* **2012**, *368* (1), 540−546.

(63) Guler, U. A.; Sarioglu, M. Removal of tetracycline from wastewater using pumice stone: equilibrium, kinetic and thermodynamic studies. *J. Environ. Health Sci. Eng.* **2014**, *12*, 79.

(64) Mohammed, A. A.; Najim, A. A.; Al-Musawi, T. J.; Alwared, A. I. Adsorptive performance of a mixture of three nonliving algae classes for nickel remediation in synthesized wastewater. *J. Environ. Health Sci. Eng.* **2019**, *17* (2), 529−538.

(65) Umeh, C. T.; Akinyele, A. B.; Okoye, N. H.; Emmanuel, S. S.; Iwuozor, K. O.; Oyekunle, I. P.; Ocheje, J. O.; Ighalo, J. O. Recent approach in the application of nanoadsorbents for malachite green (MG) dye uptake from contaminated water: A critical review. *Environ. Nanotechnol., Monit. Manage.* **2023**, *20*, No. 100891.

(66) Wang, D.; Zhang, J.; Guo, L.; Dong, X.; Shen, H.; Fu, F. Synthesis of nano-porous Bi$_2$WO$_6$ hierarchical microcrystal with selective adsorption for cationic dyes. *Mater. Res. Bull.* **2016**, *83*, 387−395.

(67) Kumar, S.; Verma, G.; Gao, W. Y.; Niu, Z.; Wojtas, L.; Ma, S. Anionic Metal−Organic Framework for Selective Dye Removal and CO$_2$ Fixation. *Eur. J. Inorg. Chem.* **2016**, *2016*, 4373−4377.

(68) Yan, H.; Yang, L.; Yang, Z.; Yang, H.; Li, A.; Cheng, R. Preparation of chitosan/poly(acrylic acid) magnetic composite microspheres and applications in the removal of copper(II) ions from aqueous solutions. *J. Hazard. Mater.* **2012**, *229*−*230*, 371−380.

(69) Ahmadi, S.; Banach, A.; Mostafapour, F. K.; Balarak, D. Study survey of cupric oxide nanoparticles in removal efficiency of ciprofloxacin antibiotic from aqueous solution: adsorption isotherm study. *Desalin. Water Treat.* **2017**, *89*, 297−303.

(70) Magesh, N.; Annam Renita, A.; Siva, R.; Harirajan, N.; Santhosh, A. Adsorption behavior of fluoroquinolone(ciprofloxacin) using zinc oxide impregnated activated carbon prepared from jack fruit peel: Kinetics and isotherm studies. *Chemosphere* **2022**, *290*, 1−10.

(71) Shi, S.; Fan, Y.; Huang, Y. Facile low temperature hydrothermal synthesis of magnetic mesoporous carbon nanocomposite for adsorption removal of ciprofloxacin antibiotics. *Ind. Eng. Chem. Res.* **2013**, *52*, 2604−2612.

(72) Khoshnamvand, N.; Ahmadi, S.; Mostafapour, F. K. Kinetic and isotherm studies on ciprofloxacin an adsorption using magnesium oxide nanopartices. *J. Appl. Pharm. Sci.* **2017**, *7* (11), 79−83.

(73) Peñafiel, M. E.; Vanegas, E.; Bermejo, D.; Matesanz, J. M.; Ormad, M. P. Organic residues as adsorbent for the removal of ciprofloxacin from aqueous solution. *Hyperfine Interact.* **2019**, *240*, 1−13.

(74) Olawale, M. D.; Tella, A. C.; Obaleye, J. A.; Olatunji, J. S. Synthesis, characterization and crystal structure of a copper-glutamate metal organic framework (MOF) and its adsorptive removal of ciprofloxacin drug from aqueous solution. *New J. Chem.* **2020**, *44* (10), 3961−3969.

(75) Mohammed, A. A.; Tariq, J. A.-M.; Sabreen, L. K.; Mansur, Z.; Alaa, M. Al-M. Simultaneous adsorption of tetracycline, amoxicillin, and ciprofloxacin by pistachio shell powder coated with zinc oxide nanoparticles. *Arabian J. Chem.* **2020**, *13*, 4629−4643.

(76) Rahdar, S.; Rahdar, A.; Igwegbe, C. A.; Moghaddam, F.; Ahmadi, S. Synthesis and physical characterization of nickel oxide nanoparticles and its application study in the removal of ciprofloxacin from contaminated water by adsorption: Equilibrium and kinetic studies. *Desalin. Water Treat.* **2019**, *141*, 386−393.

(77) Fei, Y.; Li, Y.; Han, S.; Ma, J. Adsorptive removal of ciprofloxacin by sodium alginate/graphene oxide composite beads from aqueous solution. *J. Colloid Interface Sci.* **2016**, *484*, 196−204.

(78) Ma, W.; Dai, J.; Dai, X.; Yan, Y. Preparation and characterization of chitosan/kaolin/Fe3O4 magnetic microspheres and their application for the removal of ciprofloxacin. *Adsorpt. Sci. Technol.* **2014**, *32* (10), 775−790.

(79) Li, X.; Wang, W.; Dou, J.; Gao, J.; Chen, S.; Quan, X.; Zhao, H. Dynamic adsorption of ciprofloxacin on carbon nanofibers: quantitative measurement by in situ fluorescence. *J. Water Process Eng.* **2016**, *9*, e14−e20.

(80) Arya, V.; Philip, L. Adsorption of pharmaceuticals in water using Fe$_3$O$_4$ coated polymer clay composite. *Microporous Mesoporous Mater.* **2016**, *232*, 273−280.

(81) Umeh, C. T.; Asegbeloyin, J. N.; Akpomie, K. G.; Oyeka, E. E.; Ochonogor, A. E. Adsorption properties of tropical soils from Awka North Anambra Nigeria for lead and cadmium ions from aqueous media. *Chem. Afr.* **2020**, *3*, 199−210.

(82) Umeh, T. C.; Nduka, J. K.; Akpomie, K. G. Kinetics and isotherm modeling of Pb (II) and Cd(II) sequestration from polluted water onto tropical ultisol obtained from Enugu Nigeria. *Appl. Water Sci.* **2021**, *11*, 65.

(83) Yadav, S.; Asthana, A.; Singh, A. K.; Chakraborty, R.; Vidya, S. S.; Susan, M. A. B. H.; Carabineiro, S. A. C. Adsorption of cationic dyes, drugs and metal from aqueous solutions using a polymer composite of magnetic/β-cyclodextrin/activated charcoal/Na alginate: Isotherm, kinetics and regeneration studies. *J. Hazard. Mater.* **2021**, *409*, No. 124840.

(84) Ai, Y.; Liu, Y.; Huo, Y.; et al. Insights into the adsorption mechanism and dynamic behavior of tetracycline antibiotics on reduced graphene oxide (RGO) and graphene oxide (GO) materials. *Environ. Sci.: Nano* **2019**, *6*, 3336−3348.

(85) Yilmaz, M.; Al-Musawi, T. J.; Saloot, M. K. Synthesis of activated carbon from Lemna minor plant and magnetized with iron(III) oxide magnetic nanoparticles and its application in removal of Ciprofloxacin. *Biomass Convers. Biorefin.* **2022**, *14*, 649−662.

(86) Ma, J.; Xiong, Y.; Dai, X. Adsorption behavior and mechanism of ciprofloxacin and Cu(II) on graphene hydrogel wetted surface. *Chem. Eng. J.* **2020**, *380*, No. 122387.

(87) Li, J.; Zhang, K.; Zhang, H. Adsorption of antibiotics on microplastics. *Environ. Pollut.* **2018**, *237*, 460−467.

(88) Carole, S.; Quelen, L. S.-B.; Marcela, F. S.; Marcelo, F. V.; Rosângela, B. Development of an activated carbon impregnation process with iron oxide nanoparticles by green synthesis for diclofenac adsorption. *Environ. Sci. Pollut. Res.* **2019**, *27*, 6088−6102.

(89) Nduka, J. K. Application of Chemically Modified and Unmodified Waste Biological Sorbents in Treatment of Wastewater. *Int. J. Chem. Eng.* **2012**, 1−7.

(90) John, I. I.; Akinpelu, K. B.; Titus, C. E.; Congrui, G. J.; Saheed, M.; Adeyinka, S. Y.; Virendra, K. Y.; Chinenye, I. Treated Kaolin Clay Incorporated with Nickel Nanoparticles for Enhanced Removal of Crystal Violet and Methyl Orange from Textile Wastewater. *Appl. Eng. Mater.* **2024**, *2*, 1031−1046.

(91) Pei, Y.-Y.; Guo, D.-M.; An, Q.-D.; Xiao, Z.-Y.; Zhai, S.-R.; Zhai, B. Hydrogels with diffusion-facilitated porous network for improved adsorption performance. *Korean J. Chem. Eng.* **2018**, *35*, 2384−2393.

(92) An, Y.; Zheng, H.; Sun, Q.; Zheng, X.; Liu, W.; Tang, X.; Xiong, Z. Two-step synthesis of a single-layer grafting self-floating adsorbent for anionic dyes adsorption, surface separation and concentration. *J. Hazard. Mater.* **2020**, *384*, No. 121262.

(93) Rajapaksha, A. U.; Chen, S. S.; Tsang, D. C. W.; Zhang, M.; Vithanage, M.; Mandal, S.; Gao, B.; Bolan, N. S.; Ok, Y. S. Engineered/designer biochar for contaminant removal/immobilization from soil and water: Potential and implication of biochar modification. *Chemosphere* **2016**, *148*, 276−291.

(94) Singh, S.; Kumar, V.; Datta, S.; Dhanjal, D. S.; Sharma, K.; Samuel, J.; Singh, J. Current advancement and future prospect of biosorbents for bioremediation. *Sci. Total Environ.* **2020**, *709*, No. 135895.

(95) Christopher, C. O.; Matthew, N. A.; Paschal, E. O.; Chijioke, E. O.; Joseph, T. N.; Chinenye, A. I.; Toochukwu, T. K.; Ikenna, H. O. Adsorption of antibiotics from aqueous media using nanocomposites: Insight into the current status and future perspectives, review. *Chem. Eng. J.* **2024**, *497*, No. 154767.

(96) Zhao, Y.; Liu, F.; Qin, X. Adsorption of diclofenac onto goethite: adsorption kinetics and effects of pH. *Chemosphere* **2017**, *180*, 373−378.

(97) Qin, Y.; Luo, J.; Zhao, Y.; Yao, C.; Li, Y.; An, Q.; Xiao, Z.; Zhai, S. Dual-wastes derived biochar with tailored surface features for highly efficient p-nitrophenol adsorption. *J. Cleaner Prod.* **2022**, *353*, No. 131571.